Nomadic Planets Near the Solar System

T. Marshall Eubanks*

Asteroid Initiatives LLC, Clifton, Virginia, USA

Abstract

Gravitational microlensing has revealed an extensive population of "nomadic" planets not orbiting any star, with Jupiter-mass nomads being more populous than main sequence stars. Except for distant objects discovered through microlensing, and hot, young nomads found near star formation regions, to date only a small number of nomad candidates have been discovered. Here I show that there should be significant numbers of mature nomadic exoplanets close enough to be discovered with existing or planned astronomical resources, including dozens to hundreds of planets closer than the nearest star. Observational data are used to derive models relating mass, radius, heat flux and magnetic dipole moment; these are used together with population density models to show the observability of nomads in the IR, due to thermal emissions, and at radio frequencies, due to cyclotron maser instabilities. These neighboring nomadic planets will provide a new exoplanet population for astronomical research and, eventually, direct exploration by spacecraft.

Keywords: `planetary discovery, nomadic planets, exoplanets, brown dwarfs`

1. Introduction

Although the concept of nomadic exoplanets[1] (also called rogue planets) has a fairly long history [1, 2], they were only firmly detected relatively recently. No-

*Corresponding author. Tel.: +1-703-341-9672
Email address: `tme@asteroidinitiatives.com` (T. Marshall Eubanks)

madic planets young enough to remain hot ($\gtrsim$ 1000 K) are likely to be found near the site of their formation, and the first nomads were found in star formation regions as a result of near-InfraRed (near-IR) searches [3]. Gravitational microlensing is in principle well suited for the discovery of a galactic population of older, colder, nomads, but the expected duration of lensing events in the galactic bulge is $\sim$1.5 $\sqrt{M/M_{Jupiter}}$ days for a lens of mass M, and early microlensing surveys of bulge stars did not have a sufficiently high cadence to reliably detect the brief events expected from Jupiter-mass nomads. Mature (cool) nomadic planets were thus first firmly detected in the 2006-2007 microlensing data from the MOA-II survey, with cadences of 10 to 50 min [4]. These microlensing observations show that nomadic Jupiter-mass planets are more common than main sequence stars, implying a population of nomads closer than the nearest stars. A few nomads have recently been discovered relatively near the Sun, but they are mostly fairly young and warm objects [5, 6]. A very recent discovery [7], WISE J085510.83-071442.5 (or W0855), the coldest known brown dwarf or exoplanet, with an effective temperature of 235–260 K and a parallax distance of only 7.58 $\pm$ 0.26 ly [8], is a candidate member of the set of neighboring nomadic exoplanets discussed in this paper.

Sumi *et al.*[4] used microlensing data to estimate the ratio of the number density of Jupiter-mass unbound exoplanets, n_J, and the number density of main sequence stars $n_\star$, yielding an estimate n_J / $n_\star$ = $1.9^{+1.3}_{-0.8}$ for their power law model. The stellar number density is well known from luminosity data [9], yielding an estimate for n_J,

$$n_J = (6.7^{+6.4}_{-3.0}) \times 10^{-3}\,\mathrm{ly}^{-3} \quad (1)$$

and thus an estimate for the expected mean distance to the nearest Jupiter mass

[1]This paper defines a nomadic planet, or nomad, as any exoplanet not bound to a star, an exoplanet as any condensed normal matter object outside the solar system with a mass, M, $\geq$ the Lunar mass, M_{Moon} and $\leq$ the deuterium burning limit of 13 times the mass of Jupiter, $M_{Jupiter}$, and a brown dwarf as any such object with a mass such that 13 $M_{Jupiter}$ < M $\leq$ 65 $M_{Jupiter}$, the hydrogen burning limit.

nomadic planet, D_J, with

$$D_J = 3.28^{+0.7}_{-0.6}\,\mathrm{ly}\ , \tag{2}$$

the mean minimum distance being ∼77% of the distance to Proxima Centauri.

While the nearest nomadic planets will be close enough for intensive study, they should also sample conditions of planetary formation throughout the galaxy. Recent work shows that stars migrate throughout the Galaxy after their formation [10]; nearby nomadic planets can similarly be expected to participate in widespread migrations and thus should come from throughout the galaxy. The nearby nomadic planets will also sample the varieties of planetary evolution. Nomads could be "native," forming outside any star system, or "stellar," ejected from their birth stellar system by a variety of mechanisms, including by scattering during planetary formation, by scattering or galactic tides during their host star's main sequence phase, or by being shed as a result of stellar mass loss after their host leaves the main sequence [11]. The primary sources of nomadic planets remain unclear, but as planet-planet scattering and post-main sequence shedding certainly should produce nomads but even together are apparently insufficient to explain the observed nomadic number density [12], there is likely to be a significant population of both stellar and native nomads close to the solar system.

The population density of the nomad exoplanets is sufficiently large (see Section 2) that there are good prospects of discovering at least the more massive close bodies (roughly of the mass of Saturn or larger) through observation of either their IR thermal (Sections 3 and 4) or their radio maser-cyclotron emissions (Sections 5 and 6). As is discussed in Section 7, while discovering neighboring nomads through microlensing is unlikely with current technology, due to the very low optical depth and brief durations expected for these events, the post-discovery prediction and observation of microlensing events by nearby nomads should play an important role in their study, by providing a means for the direct determinations of their masses. Finally, Section 8 describes how the close nomadic planets, despite their cold exteriors, could be possible locations

for both active and fossil biologies, and thus are likely to provide the closest objects of astrobiological interest outside of our own solar system.

2. The Number Density of Nomadic Exoplanets

The number density model used in this paper is combination of two power laws [4, 13], with the nomadic planet (nm) model being

$$\frac{dn_{nm}}{dM} = \kappa_{nm} M^{-\alpha_{nm}} \ , \tag{3}$$

where n_{nm} is the number density (in units of ly^{-3}) for a planet of mass M, κ_{nm} is a constant, set by the number of Jupiter mass nomads, and α_{nm} the power law exponent. A similar equation, with different numerical values, is used for the brown dwarf (bd) density. This and subsequent calculations assume that nomadic planets and brown dwarfs are distributed randomly in space (following a 3-dimensional Poisson distribution), that their number density does not depend on location in the Galactic disk, and that the combined number density is continuous at 13 $M_{Jupiter}$. I also assume the "Jupiter-mass object" number ratio of Equation 1 corresponds to a number density integral about a decade in mass logarithmically centered on 1 $M_{Jupiter}$ (i.e., an integral over $M_{Jupiter}/\sqrt{10} \leq M < \sqrt{10}\ M_{Jupiter}$); plots and estimates in this paper based on object number densities are unless otherwise stated likewise are based on integrals over a decade in mass centered on the reporting value. (Note that for $M > 4.1\ M_{Jupiter}$ estimates averaged over a decade in mass include a contribution from the brown dwarf distribution.)

The Sumi *et al.* estimate for the power law exponents are

$$\alpha_{mn} = 1.3^{+0.3}_{-0.4} \ . \tag{4}$$

for the nomadic planets and

$$\alpha_{bd} = 0.48^{+0.24}_{-0.27} \ . \tag{5}$$

for the brown dwarfs. A strong anticorrelation was reported [13] between the estimates of α_{mn} and α_{bd}; this was assumed to be = -1 in calculating errors.

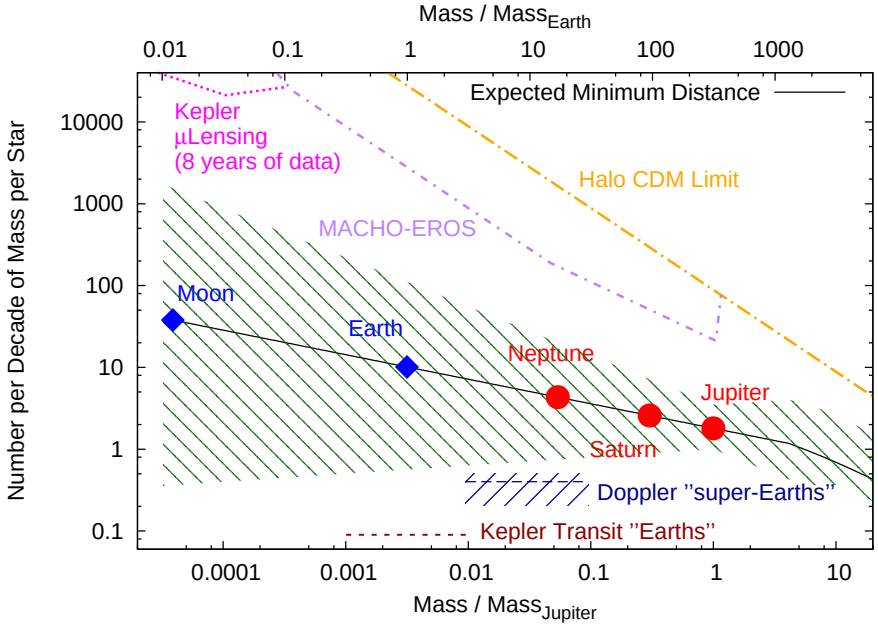

Figure 1: The nomadic planet number density per decade of mass compared to the total galactic stellar density (central curve, with cross-hatching of formal errors). The two lower curves are estimates of the fraction of stars with an orbiting Earth or super-Earth, while the upper curves are upper bounds of the number density, from Galactic kinematics (the halo CDM limit) and from gravitational microlensing from the ground-based MACHO-EROS surveys. The Kepler microlensing limit are a prediction of the limit possible with a nominal 8 year mission. (The mean values for the objects with the masses of solar system objects are shown here and in Figure 2 as a convenience to the reader.)

The scale of the brown dwarf distribution is set by the finding [14] that the total number of hydrogen-burning stars outnumber brown dwarfs by a factor of ∼6. Equations 3 and 4 were applied between the mass of the Moon (4×10^{-5} $M_{Jupiter}$) and the Deuterium burning limit (∼13 $M_{Jupiter}$), with the brown dwarf power law extending the number density model up to 65 $M_{Jupiter}$.

Figure 1 shows the integrated number density for the entire nomadic planet mass range, relative to the total main sequence number density, together with the error derived from the quoted formal errors (displayed as the right-sloping cross-hatching). Independent upper bounds of the number density of compact

objects of any sort are provided by the additional curves above the number density estimate in Figure 1. The halo Cold Dark Matter (CDM) curve is derived assuming that the entire Galactic halo dark matter density, as estimated using stellar kinematics [15], is due to compact objects of the given mass, while the MACHO+EROS constraints are from ground-based optical microlensing observations [16]. These independent gravitational lensing constraints indicate that there cannot be more than ∼1000 Earth-mass nomads per star, and thus that α_{nm} is $\lesssim 2.2$.

The two horizontal lines below the hatched number density curve are estimates of the density of exoplanets in stellar orbits, from Kepler transit discoveries of Earth-mass planets (the lower dashed line) [17] and ground based radial velocity discoveries of super-Earths for M $\sin$ i = 3 to 30 times the mass of the Earth, M_{Earth}, where i is the unknown inclination of the Doppler-discovered exoplanet (slightly above and to the right of the Kepler estimate) [18]. These estimates surprisingly appear to indicate that Earths and super-Earths are more likely to be nomads than in stellar orbits; more probably this simply reflects observational biases due to the difficulty of discovering small planets and planets with long orbital periods.

Figure 2 shows the expected minimum distance, R_{min}, as a function of nomad mass. The nearest "dark-Jupiter" should be considerably closer than Proxima Centauri, and there should thus be a few Jupiter-mass nomads within the distance to that star. Luhman[19] used IR data from the WISE space telescope data to bound the minimum distance to solar companions with the mass of Jupiter and Saturn. These limits, shown at the bottom of Figure 2, would also apply to mature nomadic planets of roughly the solar age, and are consistent with the expected minimum distances to such bodies. The expected minimum distances of brown dwarfs are, by comparison, considerably larger, and it is statistically unlikely that there are many (if any) brown dwarfs closer than the recently discovered Luhman 16 binary [20] (shown at the top right).

In order to predict the number densities of nomadic exoplanets with masses much smaller than that of Jupiter it is necessary to extrapolate the power law

density models into mass regimes not yet well constrained by microlensing [13], leading to the three order of magnitude uncertainty in the number density of Earth-mass nomads in Figure 1 and the factor of almost 6 uncertainty in the distance to the nearest Earth-mass nomad seen in Figure 2. This uncertainty is driven by the uncertainty in α_{nm}, which is sufficiently large that it is not clear whether the nomadic planet number distribution is dominated by the smallest or the largest bodies, i.e., whether $\alpha_{nm} > 1$, as is the case for stars and for the larger Kuiper Belt Objects [13], or is ≤ 1, as is the case for Brown Dwarfs, with $\alpha_{bd} \sim 1/2$. Reducing the uncertainty in α_{nm} could be done by extending the gravitational lensing detection of nomadic exoplanets to lower masses, ideally down to lenses with the mass of the Earth or smaller.

An Earth-mass gravitational lensing event in the galactic bulge would have a typical duration of $\sim$2 hours; microlensing surveys with cadences of minutes are thus required to significantly bound the galactic population of Earth-mass nomads with gravitational lensing. The Kepler space telescope survey for transiting planets has a cadence of 30 minutes; these data usefully limit the microlensing rate of halo MACHO objects in the mass range from $\sim$0.002 to $\sim$0.1 M_{Earth} [21]. Kepler, however, only observes $\sim$150,000 stars at one time, closer, and thus with a lower optical depth for microlensing, than the bulge stars typically used in microlensing surveys; even a full 8 years of Kepler mission data (see Figure 1) would not be sufficient to significantly bound the population density predicted for Earth-mass nomadic planets [22]. Improved constraints on the galactic number density of Earth-mass nomads will require either dedicated high-cadence ground based surveys [23] or a new generation of space-based microlensing surveys [24].

3. Thermal Modeling of Nomadic Planets

Nearby nomadic planets are likely to have the same age range as nearby stars, from $\lesssim$ 1 Gyr to as old as the Galactic disk itself (8.8 $\pm$ 1.7 Gyr) [25, 26]; nearby nomadic halo planets could be even older. The models in this paper

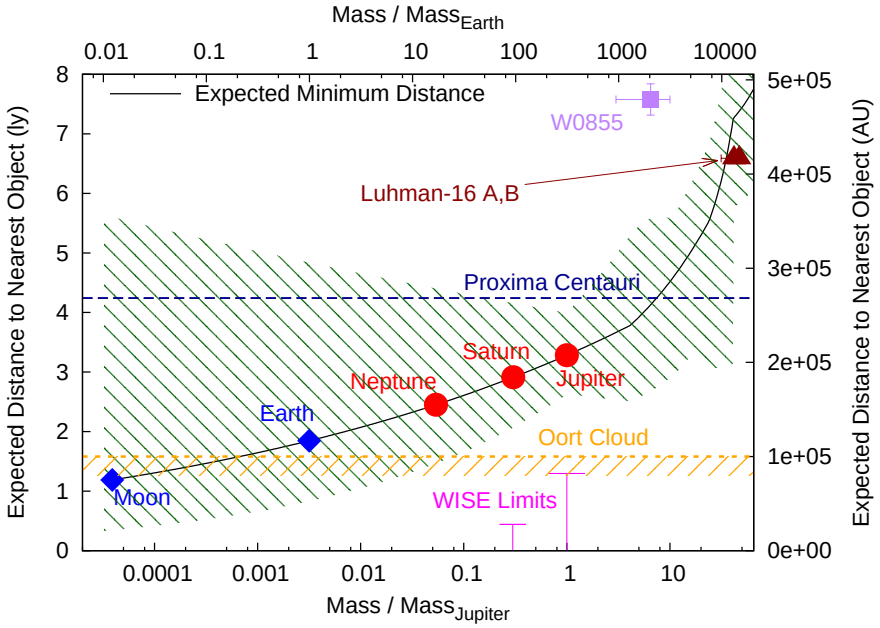

Figure 2: The expected minimum distance, R_{min}, as a function of nomadic planets mass, based on the power law number-density models derived from observations. The estimated limit of the solar system's Oort cloud of comets is shown, along with the distance to Proxima Centauri, as horizontal lines. The estimated distance and masses for the closest known brown dwarfs, the Luhman 16 binary, are also shown; these agree well with the predicted closest distances for those masses. By contrast, W0855, the cold nomadic planet WISE J085510.83-071442.5, is considerably more distant than the predicted closest distance for its mass, and so it would be reasonable to expect there would be closer nomads of similar masses. The "WISE Limits" are for mature nomadic planets (or solar companions) with the mass of Jupiter and Saturn, respectively (see text).

are intended to be conservative estimates of thermal radiation for mature nomadic exoplanets of roughly the age of the solar system. Fortney *et al.*[27] used radiative-convective models of Jupiter, Saturn, Uranus and Neptune to estimate the change in the thermal luminosities of these bodies with time, while Frank *et al.* [28] provide similar estimates for the heating of terrestrial exoplanets from changes in the production and decay of radionuclides in the galaxy. While younger nomadic planets are likely to be warmer, and thus easier to detect, than solar system bodies with the same mass, these models indicate that changes in heat production with age for planets older than $\sim$2 billion years would have relatively small effects in IR luminosity compared to the uncertainty introduced by errors in the planetary number density.

Mature nomads should be close to radiative equilibrium on their surfaces or upper cloud-tops, and will thus radiate according to their size and internal heating. Models previously derived from exoplanet data are used to estimate planetary radii as a function of mass (subsection 3.1), while solar system data are used to derive power density models (subsection 3.2), thus enabling the estimation of the IR flux of mature nomads as a function of mass. Of course, the black-body radiation models used in this paper do not account for atmospheric spectral features which can be expected to cause higher or lower luminosities at the wavelengths of various spectral lines.

3.1. Planetary Mass-Radius Relations

It is possible to simultaneously determine both the planetary mass and radius for some well-observed exoplanets (primarily those with both stellar transit and Doppler radial velocity data); the recent proliferation of exoplanet data has substantially improved knowledge of planetary radii as a function of mass, particularly for masses between the Earth and Neptune, and those larger than Jupiter, where there are no solar system analogs. Figure 3 shows the mass-radius relation for every exoplanet in the exoplanet.eu database [29] as of October 4, 2014, together with similar data for the solar system planets, the Moon, Titan and the Galilean satellites, and also for three well-studied radio-loud Ultra-Cool

brown Dwarfs (UCDs) [see 30, and Section 5]. There are different mass-radius relations for terrestrial planets and giant planets, and both these planetary types display an apparent change in their equation of state for sufficiently large masses [31].

This paper uses the models of Marcy *et al.*[32] for "terrestrial" planets (tp), those with masses roughly between M_{Moon} and 30 M_{Earth}. (Super-Earths are typically considered to have masses up to ∼10 M_{Earth}, but it is not clear what the actual upper limit is for terrestrial planet masses [33].) There is an apparent change in the mass-radius relation at R ∼1.5 R_{Earth} (or M ∼4 M_{Earth}); below that size, the density typically increases with mass, while above that size the radius is roughly ∝ mass, and the bulk density thus decreases with mass [32]. The decreasing density is thought to reflect the presence of an extended Hydrogen-Helium atmosphere for the larger bodies [34]. The Marcy *et al.* radius and density models for terrestrial planets are

$$\begin{array}{lcll} \rho_{\rm tp} & = & 2320 + 3190\ \frac{R}{R_{Earth}} & {\rm kg\,m^{-3}} \quad {\rm M} \leq 4\ {\rm M}_{Earth} \\ \frac{R}{R_{Earth}} & = & 0.345\ \times\ \frac{M}{M_{Earth}} & {\rm M} > 4\ {\rm M}_{Earth} \end{array} \tag{6}$$

These models are based on exoplanet data up to ∼4 R_{Earth} (or ∼10 M_{Earth}); the terrestrial radius model for masses > 30 M_{Earth} (indicated by the dotted line in Figure 3) is both an extrapolation and matches none of the available data, and so is not used.

Objects with roughly the solar composition and a mass between ∼1 and ∼80 $M_{Jupiter}$, which includes Jupiter and super-Jupiter mass exoplanets together with brown dwarfs and even some low mass stars, have radii close to that of Jupiter, but with a slight decline with increasing mass [31]. This paper uses the mass-radius relationship for giant planets (gg) derived using CoRoT space telescope data [35], with

$$\rho_{\rm gg} = \begin{cases} 730 & {\rm kg\,m^{-3}} \quad {\rm M} \leq {\rm M}_{Jupiter} \\ 730\ \times \left(\frac{M}{M_{Jupiter}}\right)^{1.17} & {\rm kg\,m^{-3}} \quad {\rm M} > {\rm M}_{Jupiter} \end{cases} \tag{7}$$

This curve is the dashed line in Figure 3; the transition from the constant density was chosen to begin at 1 $M_{Jupiter}$ to improve the fit to the giant planets in the

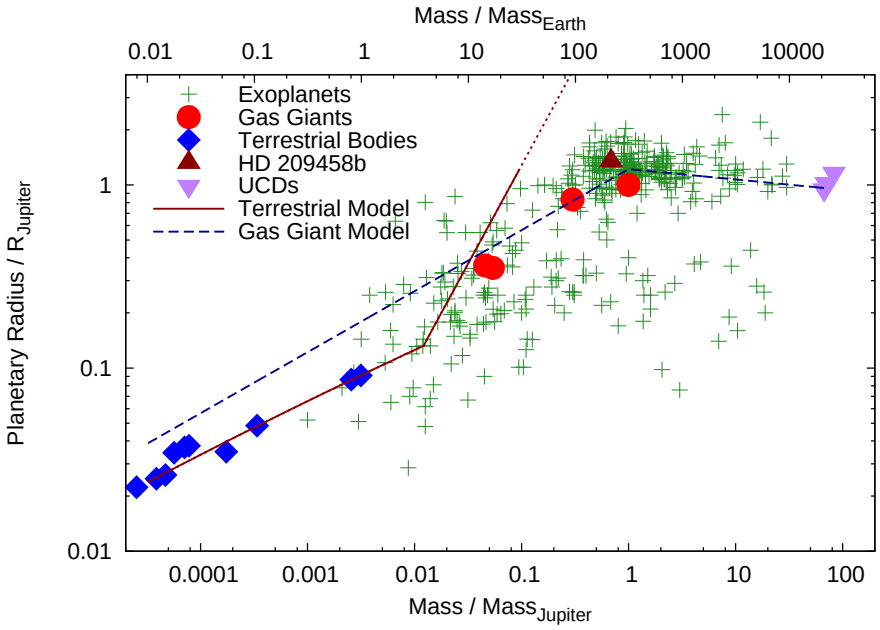

Figure 3: The planetary and UCD radius as a function of mass, for the Moon, Titan, the Galilean satellites and the 8 planets of the solar system, the 1822 exoplanets in the exoplanet.eu database as of October 4, 2014, and 3 fast rotating UCDs. The terrestrial radius model is based on exoplanet data up to ∼10 M_{Earth}; in this paper the terrestrial radius model for masses $>$ 30 M_{Earth} (indicated by the dotted line) is assumed to be unreliable and is not used.

solar system. Note that many of the discovered exoplanets are hot Jupiters orbiting close to their stars; these objects seem to be slightly inflated (with radii ∼10%–25% greater than predicted in Equation 7), and thus appear above this curve in Figure 3. The hot Jupiter HD 209458b, discussed in subsection 5.1, appears to be such an object.

3.2. Thermal Power Generation as a Function of Mass

The study of the solar system indicates that the internal heating of mature exoplanets would be dominated by energy from long-lived radioactive elements (for terrestrial planets) or from the settling of denser components towards the body's core (for the giant planets). Given the limited amount of solar system

data on internal planetary heating, and a near total absence of relevant exoplanet data, very simple models were derived assuming that internal power generation is proportional to mass for the two different planet types. (It is likely that there are other planetary types, but hopefully the two solar system types span a reasonable fraction of the actual nomadic planets.) Given models for energy density and radius, it is straightforward to compute the black body intensity as a function of wavelength for a planet of a given mass and type, estimate the maximum distance this could be detected for a given telescope sensitivity, and then to use the estimated number density to determine the probability of finding one or more such bodies within that distance.

Figure 4 shows determinations of the internal energy production for bodies in the solar system, based on direct estimates of heat flow for the Earth [36] and Moon [37], and astronomical and spacecraft observations of excess heat production for Jupiter [38], Saturn [39, 40], Uranus [41, 42] and Neptune [41, 43]. (Heat flow estimates are also available for the Galilean satellites, but these are dominated by Jovian tidal heating.) There appear to be at least two different regimes of internal power density, with the Earth and Moon having nearly the same power density (power production per unit mass), and Jupiter and Saturn having a considerably larger power density, presumably reflecting the different heat production from radionuclides and gravitational settling (see Figure 4).

A very simple model for power density, ϖ, was developed for the two planet types based on a weighted average of the available energy density estimates, yielding

$$\varpi = \begin{cases} 7.9 \times 10^{-12} & \mathrm{W\,kg^{-1}} \quad \text{terrestrial planets} \\ 1.9 \times 10^{-10} & \mathrm{W\,kg^{-1}} \quad \text{giant planets} \end{cases} \tag{8}$$

These power density models are shown as solid and dashed lines respectively in Figure 4; it is assumed in this paper that these two models bound internal power densities of nomadic planets with ages comparable to the solar system. Given an estimate for ϖ, the black body equilibrium temperatures are estimated using the Stefan-Boltzmann law and the radius and power density models of Equations 6, 7 and 8. These models imply substantial differences between the

external temperatures of super-Earths and super-Jupiters, as shown in Figure 5. The effective surface temperatures of super-Jupiters should increase strongly with mass, due to their relatively constant radii, which moves their peak emissions from the far-IR to the mid-IR for the largest nomads, while the exterior temperature of super-Earths would decrease with mass, due to their decreasing bulk densities. It is worth noting, as is discussed further in Section 8, that the actual surfaces of nomadic super-Earths, beneath thick H-He atmospheres, should increase with mass, and could be warm enough for sufficiently massive bodies to support oceans of liquid water. Although the two solar system ice giants, Uranus and Neptune, have very similar gross physical characteristics, their internal power estimates differ by at least an order of magnitude; the most recent Voyager derived estimate for the energy density of Uranus [42], although higher than a previous estimate [41], is still lower that that predicted by the terrestrial model, while the Voyager heat production estimate for Neptune is mid-way between the terrestrial and giant planet models. If the internal heat sources of the largest nomadic super-Earths are indeed similar to Uranus it will be (see Table 1 and Figure 6) very difficult to detect the thermal emissions of even the closest such bodies with existing technology, unless one happens to be significantly closer than its expected minimum distance.

4. Detecting Nearby Nomadic Planets in the Thermal InfraRed

Figure 6 displays the black body flux density expected from a set of hypothetical planets, matching in order the Earth, Uranus, Neptune, Saturn and Jupiter in mass, radius and power density, with each assumed to be at the mean closest distance for a body of its mass. A super-Jupiter with 10 times the mass of Jupiter is also included; that planet's size and power density are taken entirely from the gas giant models. Figure 6 also shows flux density limits for actual (ALMA [44], cooled WISE [45] and cooled Spitzer [46]) and planned (SPICA [47] and JWST [46]) telescopes and arrays. Table 1 provides the corresponding numerical results for these bodies. The super-Jupiter and Jupiter analogs

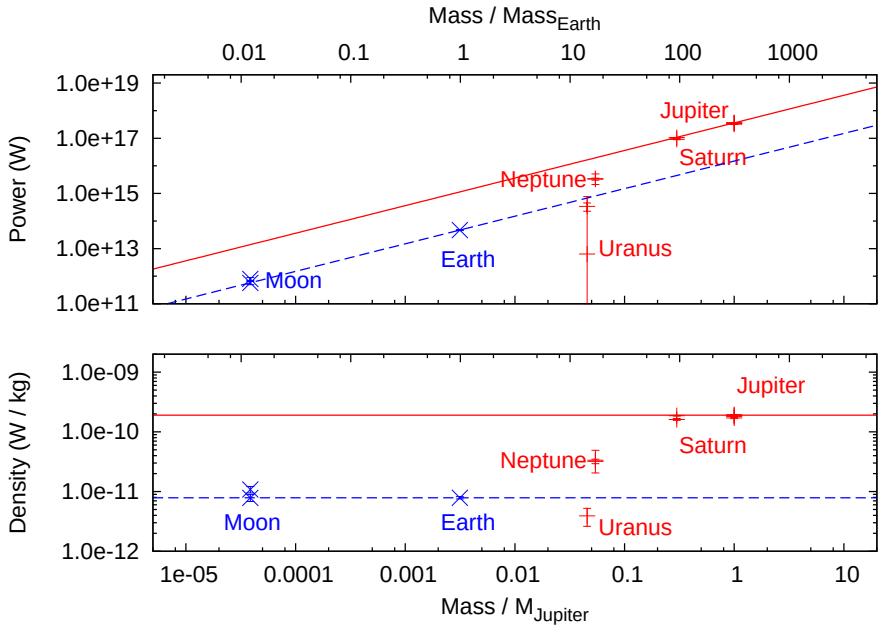

Figure 4: Internal power generation as a function of mass for total power (top) together with the power density per unit mass (bottom). The Earth and the Moon have roughly the same power density (W/kg), as do Jupiter and Saturn, but the two gas giants produce substantially more power per unit mass than do the terrestrial bodies. As a simple empirical model, terrestrial planets are assumed to share the Earth-Moon power density, while Jovian planets are assumed to share the Jupiter-Saturn power density. Note that Uranus and Neptune, although superficially similar, have considerably different power densities and do not fit either model well.

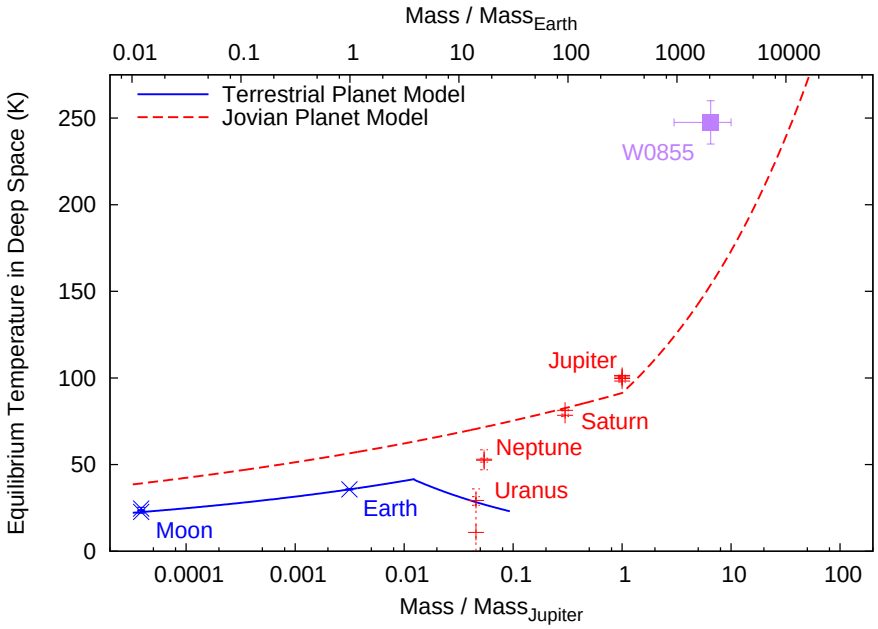

Figure 5: The equilibrium temperature in deep space due to internal power generation for mature planets far from any significant external energy sources. The terrestrial planet temperature model assumes a density implied by Equation 6; the Giant planet model assumes the densities implied by Equation 7. The values for the various solar system planets are those implied by their actual mass, radius and internal power generation. W0855 (WISE J085510.83-071442.5) is a recently discovered nomadic planet. Although it is the coldest nomad known at present, these models indicate that it is warmer than would be expected for a solar system analog. It is thus presumably either still fairly young, or the models are overly conservative for super-Jupiters.

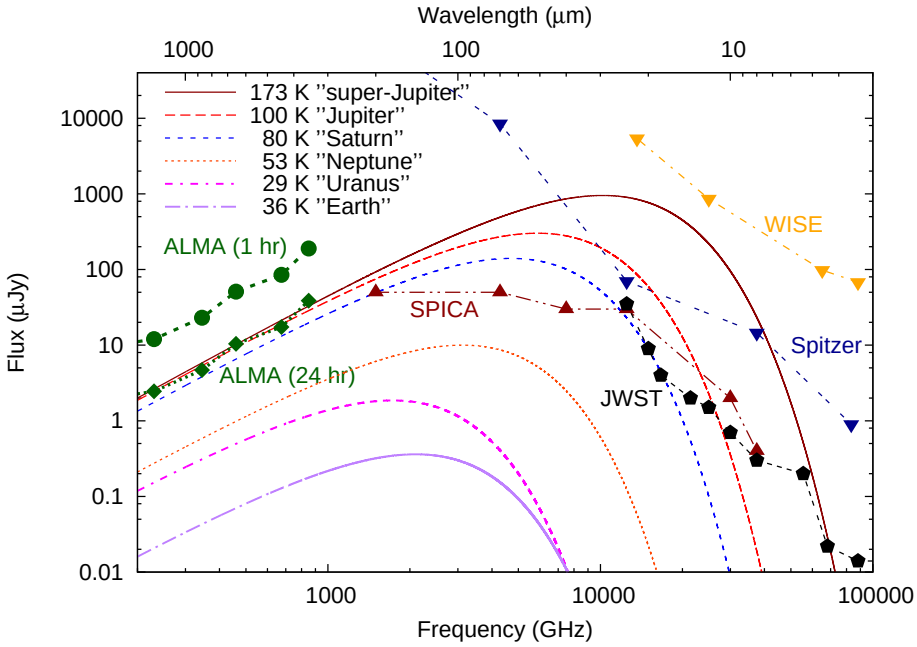

Figure 6: The IR flux density for black bodies with the same radius and internal power generation as the actual Earth, Uranus, Neptune, Saturn and Jupiter (see Table 1 and Figure 4), plus a model-derived "super-Jupiter" with a mass of 10 $M_{Jupiter}$, each with the temperature of a black body and the mean closest distance for a nomadic body of that mass (i.e., the central curve in Figure 2), together with flux density limits for various actual (ALMA, cooled Spitzer, cooled-WISE) and planned (SPICA and JWST) telescopes and arrays. (The lines connecting different channels for the various instruments are only to guide the eye.)

would be detected by five of the instruments, the Saturn analog by four, while the Uranus, Neptune and Earth analogs would not be detected by any of them.

Similar insights can be obtained by examining the flux density as a function of mass for the observing frequencies of various instruments. Figures 7, 8 and 9 show black body flux density estimates as a function of mass at 440 μm (675 GHz), 70 μm and 18 μm, representative channels of ALMA, SPICA and JWST, respectively, together with flux limits for those instruments. Despite the different wavelengths and instruments, for all of these it should be possible to detect the closest giants down to or somewhat below the mass of Jupiter, but these instruments are unlikely to discover terrestrial nomads. Table 1 shows

that Jupiter mass nomads could be detected out to ∼10 ly by SPICA at 70 μm or JWST at 18 μm, implying that a few dozens should be discoverable, while possibly hundreds of super-Jupiters could be discovered within a range of a few dozens of ly by the JWST at 10 μm.

It is thus certainly possible that there will be serendipitous IR detections of nearby giant planet nomads, and it seems likely that if such bodies are found, by whatever means, it would be possible to confirm their discovery by observations of their thermal emissions. On the other hand, the discovery of a significant fraction of these bodies in the IR would require a full-sky survey more sensitive than any yet performed, and there are apparently no near-term plans for such surveys. Fortunately, as is discussed in Section 5, it may be possible to find a substantial fraction of neighboring giant nomadic planets from the ground through observations of their non-thermal radio emissions.

5. Cyclotron Maser Radio Emissions from Nomadic Exoplanets

A completely different means of discovering magnetized nomadic planets is through the detection of their non-thermal radio emissions, generated by the electron Cyclotron Maser Instability (CMI). The strongly magnetized bodies in the solar system (the Earth plus the 4 giant planets) are all strong non-thermal radio emitters, with Jupiter at times having a greater luminosity than the Sun at frequencies between 10–40 MHz (the so-called "High Frequency," or HF, band). The CMI is the primary source of this intense decametric radiation; CMI emissions are generated by a body moving through a plasma (such as the moon Io orbiting in the rotating Jovian field), with either the body or the plasma, or both, possessing a significant magnetic field [48, 49, 50], or even from the rapid rotation of a magnetized body [30]. Such emissions provide a non-thermal means of detecting magnetized exoplanets [51], including magnetized nomads [52]. In the solar system, 5 of the 8 planets (and all of the giant planets) have a magnetic field strong enough to create a "motional" CMI, driven by the blockage of the solar wind by the planetary magnetosphere, while Jupiter (one

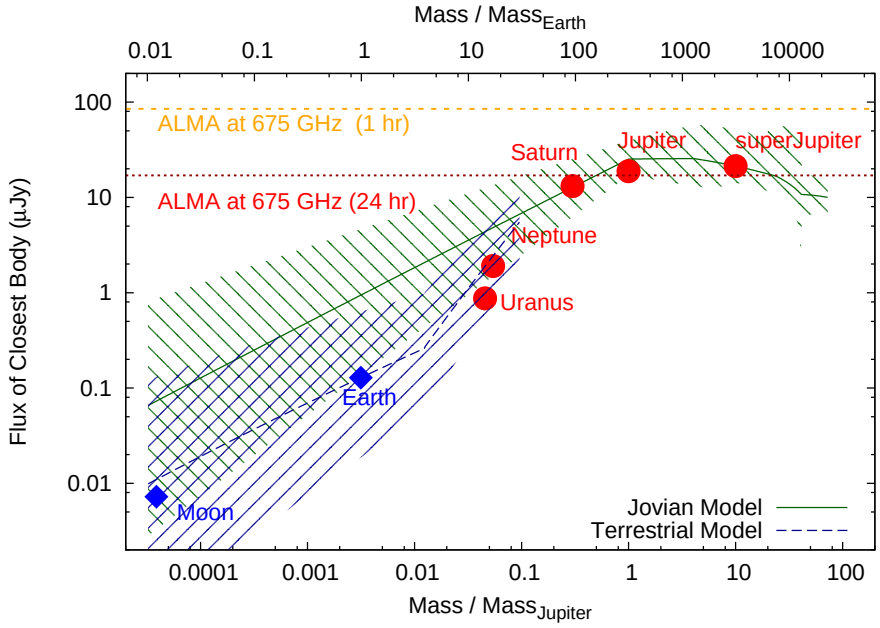

Figure 7: The thermal flux density at 675 GHz (440 μm) as a function of mass for nomadic exoplanets at their expected minimum distance, compared to the estimated sensitivity of the ALMA array at that frequency [44]. While short duration (1 hour) ALMA integrations are unlikely to detect nomadic exoplanets, longer (24 hour) integrations should be able to detect the closest nomadic gas with masses greater than Saturn, but not substantially less massive objects. (In this and Figures 8 and 9, the displayed flux densities for solar system objects are based on a black body with their actual internal heat generation and radius, while the flux densities for the 10 $M_{Jupiter}$ super-Jupiter are based purely on the giant planet model.)

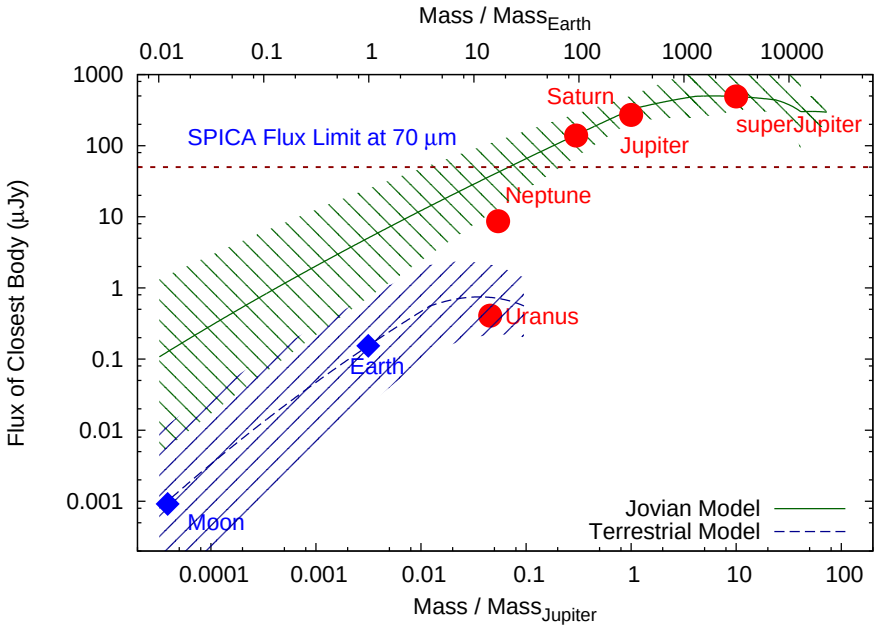

Figure 8: The thermal flux density at 70 μm as a function of mass for nomadic exoplanets at their expected minimum distance, compared with the estimated sensitivity of the 70 μm channel of the proposed SPICA space telescope (this limit is a confusion limit, not a bare flux density limit) [47]. The estimated sensitivity of SPICA at this wavelength should be able to detect the closest nomadic giant planets, but would not be able to detect nearby nomadic "super-Earths," unless they were substantially closer or warmer than expected.

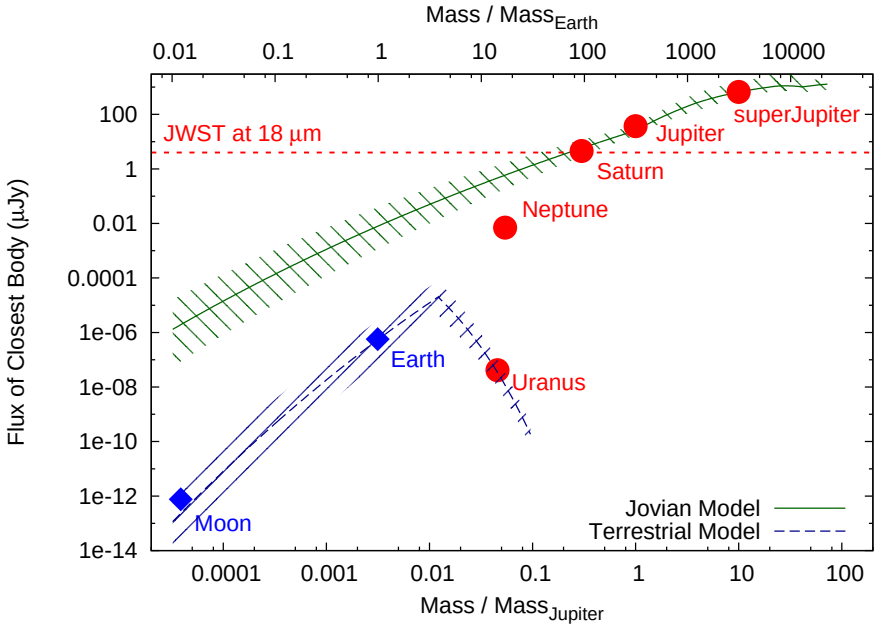

Figure 9: The thermal flux density at 18 μm as a function of mass for nomadic exoplanets at their expected minimum distance, compared with the estimated sensitivity of the 18 μm MIRI channel of the JWST space telescope (10 σ detection with 10^4 s integration) [46]. The estimated sensitivity of the JWST at this wavelength should be sufficient to detect the closest nomadic giant planets with masses $\gtrsim$ M$_{Saturn}$.

Table 1: Minimum expected distances from the best-fit microlensing population densities for analogs for solar system planets (plus a 10 $M_{Jupiter}$ "super-Jupiter"), together with the wavelength of peak flux density, the flux density at the spectral peak, and the detection range of SPICA and JWST at the given wavelength for objects of that luminosity. For the analogs of solar solar system bodies the black body model assumes the actual radius and the measured internal power generated; for the super-Jupiter the radius, temperature and thermal power are based on the giant planet model.

Object Analog	Mass	Expected R_{min}	Peak λ	Peak Flux Density at R_{min}	Detection Limit SPICA @ 70 μm	JWST @ 18 μm
	$M_{Jupiter}$	ly	μm	μJy	ly	ly
Earth	0.003	$1.85^{+2.99}_{-1.01}$	143	$0.36^{+1.41}_{-0.31}$	0.10	0.001
Uranus	0.046	$2.41^{+2.02}_{-0.99}$	173	$1.86^{+3.50}_{-1.31}$	0.22	0.0002
Neptune	0.054	$2.45^{+1.95}_{-0.99}$	96	$10.0^{+18.0}_{-6.9}$	0.42	0.10
Saturn	0.299	$2.91^{+1.24}_{-0.84}$	64	140^{+137}_{-71}	4.83	3.10
Jupiter	1	$3.28^{+0.71}_{-0.65}$	51	302^{+168}_{-98}	7.62	9.99
super-Jupiter	10	$4.52^{+1.16}_{-1.61}$	29	952^{+1357}_{-327}	14.16	58.17

quarter of the giant planets) produces an even stronger strong "unipolar" CMI radio flux, primarily due to electrons flowing through the Jupiter-Io flux tube. If these occurrence rates are typical for nomadic planets, the search for CMI emissions may provide the best near-term prospect for discovering neighboring nomadic giant planets from ground-based observations.

At present non-thermal radio emissions have not been conclusively detected from any exoplanet, stellar or nomadic [49, 51, 53], but they have been detected from brown dwarfs [54]. In particular, about 6% of the lowest mass UCDs rotate extraordinary rapidly (with periods as low as 2 hours, or ∼5 times more rapidly than Jupiter), are strongly magnetized and are intense sources of circularly polarized CMI radiation, which seems to be driven purely by their rotation [55]. (A different mechanism, heating of chromospheric plasma, is thought to drive radio and X-ray emissions from higher-mass magnetically active stars [56]; the UCD CMI sources are not strong X-ray producers.) While there are no solar system analogs for the "rotational" CMI of the rapidly rotating UCDs, it seems reasonable to assume that rapidly rotating giant planets could also generate rotational CMI, and thus could also be found by HF radio surveys. Three well-studied radio-loud UCDs, TVLM 513-46546, 2MASS J00361617+1821104 and LSR J1835+3259, [30], are used as proxies for radio-loud exoplanets in this paper.

As neither planetary dipole moments nor planetary cyclotron masers can be fully modeled from first principles, scaling relations are used to estimate emissions for arbitrary sized exoplanets [51]. Subsection 5.1 derives a double power law model for planetary magnetic moments as a function of mass and rotation period; that model plus the planetary radius is used to estimate the cyclotron frequency, $f_{cyclotron}$, as a function of mass, which determines the frequency range of CMI emissions. Subsection 5.2 describes the expected motional flux density from the motion of nomadic planets through the InterStellar Medium (ISM), while subsection 5.3 describes a combined model for unipolar and rotational flux densities based on the Jupiter-Io and UCD CMI. It should be recognized that estimates from these empirical scaling relationships are quite uncertain;

even the limited data available suggests that they will rarely be significantly more accurate than an order of magnitude.

5.1. Double Power Law Models for Magnetic Dipole Moments

This paper uses an empirical double power law dipole moment model [52, 57] to estimate the scalar dipole moment amplitude, $\mathcal{M}$ from a planet's mass, M, and rotation frequency, Ω, with

$$\mathcal{M} \sim \mathcal{M}_0 \left(\frac{M}{M_{Jupiter}} \right)^{\gamma} \left(\frac{\Omega}{\Omega_{Jupiter}} \right)^{\varepsilon} . \tag{9}$$

Figure 10 shows magnetic dipole estimates for the planets and moons of the solar system (all 8 planets plus the Moon, Io, Europa, and Ganymede), the 3 well-studied radio-loud UCDs, and a recent determination of the magnetic field for a hot Jupiter, HD 209458b [58]. The radio-loud UCDs are both more massive and faster rotating than any of the magnetized bodies in the solar system, and help span the exoplanet mass range in the absence of CMI observations of exoplanets. The magnetic dipole estimate for HD 209458b was derived from observations of Lyman α absorption near the planet [59]; the planet is a hot Jupiter and is assumed to be in synchronous rotation. The new Lyman α absorption technique for the direct determination of dipole moments, together with atmospheric circulation models for determination of rotation periods for hot Jupiters [60], should be able to considerably improve exoplanet dipole moment models in the relatively near future, particularly if they can be applied a wide range of super-Jupiter masses.

The dipole moments for three bodies (the Moon, Mars and Venus) are displayed in Figure 10 as yellow squares, denoted as "non-dipole fields." These bodies have weak fields that are not dominated by a dipole component; the dipole moment estimates for these bodies do not fit the model well and they were not included in the solution. In addition, the UCD LSR J1835+3259 was also not used in the solution as at present only an upper bound is available for its mass.

The curve in Figure 10, top, is derived from a non-linear least-squares solution for the 3 parameters of Equation 9 using mass, period and dipole moment determinations for 12 bodies, assuming formal errors equal to 60% of the measured dipole moment, while the bottom figure shows the weighted residuals from the solution. The full solution yielded $\mathcal{M}_0 = \{3.6 \pm 0.7\} \times 10^{26}$ A m^2, $\gamma = 1.52 \pm 0.06$ and $\varepsilon = 0.59 \pm 0.17$; both exponents being consistent with the default values (1.5 and 0.75, respectively) used by Vanhamäki [52]. The remainder of this paper uses these solve-for values to estimate dipole moments and related variables. Since the rotation rate of undiscovered exoplanets is unknown, in calculating properties for nomadic exoplanets I assume unless otherwise stated that each body has the same rotation rate as Jupiter.

The cyclotron frequency, $f_{cyclotron}$ is a crucial parameter for CMI observations, as it sets the upper frequency of cyclotron radio emissions. As the Earth's ionosphere has a lower transmission frequency limit of ∼10 MHz, $f_{cyclotron}$ has to be greater than that for ground-based CMI observations to be possible at all. For a given planetary radius and dipole moment, $f_{cyclotron}$ can be estimated by

$$\begin{aligned} f_{cyclotron}(M) &= \frac{eB_{polar}}{2\pi m_e} \\ &\sim \frac{e}{3\pi m_e} \frac{\mu_0 \rho \mathcal{M}_0}{M_{Jupiter}} \left(\frac{M}{M_{Jupiter}}\right)^{\gamma-1} \left(\frac{\Omega}{\Omega_{Jupiter}}\right)^{\varepsilon} \text{ Hz} \end{aligned} \tag{10}$$

(note that ρ, the planetary density, is not a constant in this Equation, but must be estimated from Equation 6 or 7, as appropriate). The $f_{cyclotron}$ resulting from the dipole moment model and Equation 10 is shown in Figure 11, together with direct estimates [48] of the frequency cutoff of maser cyclotron radiation for the magnetized bodies used in the solution. The full dipole moment solution does a reasonable job of representing the cyclotron frequencies of all the known magnetized planets except Jupiter; this is at least partially due to the model of Equation 9 under-representing the Jovian dipole moment. The "Jovian scaling" of dipole moments was developed to account for this, with $\mathcal{M}_0$ simply being set to $\mathcal{M}_{Jupiter}$. This is displayed in Figure 11 by the upper dashed curve, and appears to provide a more reasonable estimate for $f_{cyclotron}$ for Jupiter and the radio-loud UCDs. Note, however, that even using the full Jovian dipole

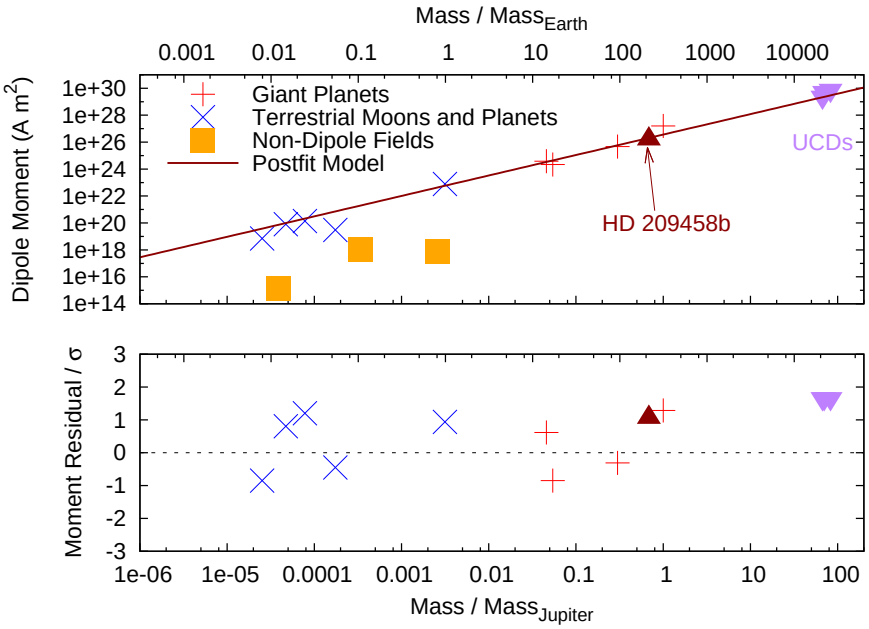

Figure 10: The dipole moments for the solar system bodies, exoplanet and three fast UCDs discussed in the text, together with the postfix power law model derived using the data for these bodies and Equation 9 (top), together with the residuals from that fit, normalized by the formal errors (bottom). Note that the double power law model includes a scaling with rotation period; the measured rotation frequency is used for the residual calculations for each body, but is set to that of Jupiter's for the curve marked "postfit model" in the upper plot. The simple double-power law model fits the available dipole data to better than an order of magnitude over a range of of magnitude of mass and 3 orders of magnitude of rotation frequency.

moment, Jupiter's cyclotron frequency is still about a factor of two larger than Equation 10 predicts [52].

Equation 10 and Figure 11 show that even with the Jovian scaling for $f_{cyclotron}$ only giant planets with M $\gtrsim$0.1 $M_{Jupiter}$ would have CMI emissions observable from the ground, with the CMI cut-off frequencies for super-Jupiters extending up to ∼350 MHz for the normal $f_{cyclotron}$ scaling (which would make such objects observable with the proposed Square Kilometer Array) and ∼1800 MHz for the Jupiter scaling (which would bring these objects within reach of radio burst surveys at 1.4 GHz, as is discussed in subsection 6.2).

UCDs have radii close to that of Jupiter's and very strong surface fields, up to 0.1 T or more; these bodies thus should have cyclotron frequencies of ∼10 GHz, considerably higher than Jupiter's. Although both the upper and lower limits of UCD CMI emissions are at present unknown, UCD burst emissions have been detected at frequencies as high as 8.4 GHz [61], which sets a lower bound on the UCD cyclotron frequency. In contrast, the hot Jupiter HD 209458b has a sufficiently low dipole moment and large radius that its predicted cyclotron frequency is well below the terrestrial cut-off frequency; it is thus not surprising that CMI emissions were not detected from this body in a sensitive search at 150 MHz [62].

For terrestrial planets $f_{cyclotron}$ appears to rapidly decline with mass for masses $\gtrsim$ 4 M_{Earth}, as the terrestrial exoplanet radius scales roughly $\propto$ mass in this mass range. If this decline actually occurs, there is little prospect of observing CMI emissions from terrestrial exoplanets from the ground; detection of radio emissions from nomadic Earths and super-Earths will thus have to wait for the development of sensitive low-frequency radio instruments in space, such as the arrays proposed (to avoid terrestrial interference) for the far-side or polar regions of the Moon [63].

5.2. Motional Maser Cyclotron Emissions From the InterStellar Medium

The motional CMI emissions in the solar system are powered from the displacement of the solar wind by a planetary magnetosphere, which results in the

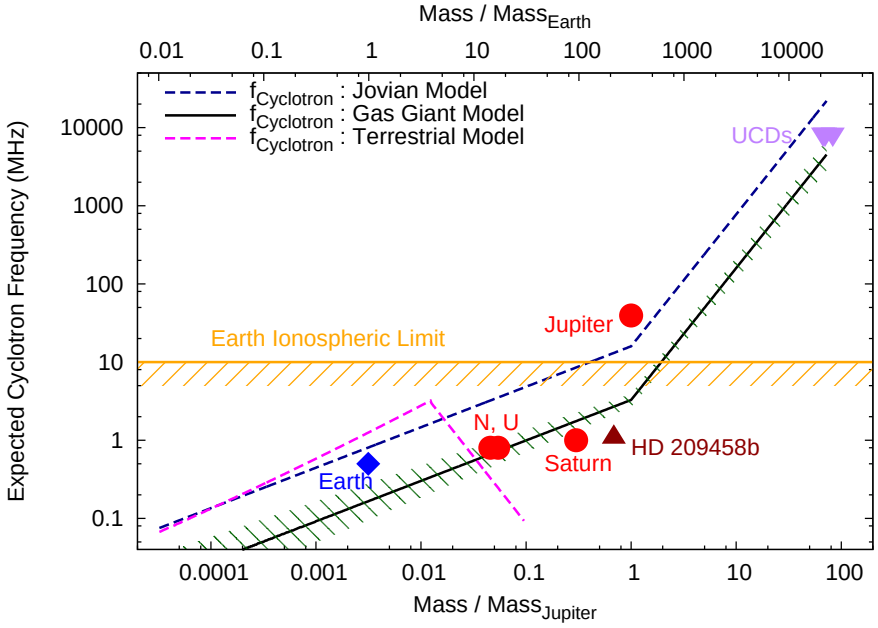

Figure 11: Estimated cyclotron frequency as a function of mass, from Equation 10, using the dipole moment scaling of Equation 9, assuming the Jovian rotation period in the dipole moment models. The individual points for solar system objects are based on the peak radio frequency of their CMI emissions (the points for Neptune and Uranus are denoted as "N, U" as they overlap). CMI emissions have not been observed from HD 209458b and so there is no direct estimate of its cyclotron frequency; the value plotted here is estimated from the measured radius and magnetic dipole moment for that body. The UCD data points are lower bounds, as the peak CMI frequencies for these bodies have not yet been found. Figure 10 shows that the Jovian dipole moment is underrepresented in the dipole moment model, and the giant planet model cyclotron frequency is thus below the well-determined Jovian cyclotron frequency of ∼39.5 MHz by a factor of ∼12. The "Jovian scaling" for $f_{cyclotron}$, which uses Equation 10 scaled to match the actual dipole moment of Jupiter, is also shown.

conversion of a small fraction of the energy of the impinging plasma into radio emissions; scaling relations have been derived to estimate the emitted power as a function of the area of the magnetosphere and the velocity and density of the solar wind at the planet's location [51]. The same mechanism should produce radio emissions from magnetized nomadic planets, powered by the relative velocity of the ISM and the planet. The ISM is thought to be nearly stationary in a rest frame moving with the mean galactic rotation, so that the relative velocity, δV, will be dominated by the peculiar velocity of the exoplanet relative to the rotating galactic rest frame [52].

Peculiar velocities of galactic disk objects in the solar neighborhood are of order 30 km s^{-1}, while nomadic exoplanets from the galactic halo would have considerably larger relative velocities, of order $\sim$340 km s^{-1}, and also a larger relative velocity scatter [64]. This higher velocity means that motional CMI emission power would be typically an order of magnitude stronger from halo nomads than from disk nomads; even if the number density of halo nomads is significantly lower than that of disk nomads, their motional CMI emissions may be more readily detectable. In the absence of direct limits for the relative proportions of these two nomad populations, the estimated flux densities are bounded in this paper by assuming that the entire nomadic planet population is either from the disk or from the halo.

Motional maser cyclotron emissions result from the conversion of the energy in the local plasma, with the power assumed to be simply related to the size of the planetary magnetosphere, R_m, by

$$P_{motional} = \beta \pi R_m^2 \delta V p_m \, \mathrm{W} \tag{11}$$

where β is a conversion efficiency [65], thought to be of order 10^{-2}, and p_m is the magnetic pressure of the ISM plasma [52], reasonably thought to dominate over or at least be comparable to the thermal and dynamic pressures, with

$$p_m = \frac{B_{ISM}^2}{2\mu_0} \, \mathrm{Pa} \ , \tag{12}$$

where B_{ISM}, the external magnetic field strength, is of order 5×10^{-10} T in

the "local cloud" of the ISM. The size of the magnetosphere itself depends on a balance of the external and the internal pressure, $p_{internal}$, generated by the planetary magnetic field, with

$$p_m = \frac{B_{ISM}^2}{2\mu_0} \sim p_{internal} = \frac{\mu_0 f_0^2 \mathcal{M}^2}{8\pi^2 R_m^6} \text{ Pa} \ , \tag{13}$$

where f_0 is a form factor thought to be ∼1.16 [52]. Equations 9 and 13 can be used to solve for R_m, and thus to determine $P_{motional}$ for an arbitrary nomadic planet mass,

$$\begin{aligned} P_{motional} \quad = \quad & \beta \delta V \left(\frac{\pi B_{ISM}^4 f_0^2 \mathcal{M}_0^2}{32\mu_0} \right)^{1/3} \times \\ & \left(\frac{M}{M_{Jupiter}} \right)^{\frac{2\gamma}{3}} \left(\frac{\Omega}{\Omega_{Jupiter}} \right)^{\frac{2\varepsilon}{3}} \text{ W} \end{aligned} \tag{14}$$

Power estimates from this Equation are converted into flux density estimates for a given distance by assuming a total emission bandwidth (∼50% of $f_{cyclotron}$) [52] and a beaming factor (∼1.6 sr) [30].

5.3. Unipolar and Rotational Radio Emissions from Nomadic Planets

There is a possibility of strong unipolar CMI emissions from nomadic planets with a suitably large moons inside their magnetospheres [52], and also for rotational CMI emissions for bodies with a sufficiently high rotational frequency [55]. For Jupiter, the Io-related Decametric radiation (Io-DAM) is both stronger and extends to higher frequencies than the Jovian Hectometric Radiation (HOM); the Jupiter Io-DAM are the strongest radio emissions from Jupiter, with an ∼30 MHz emission bandwidth [50], a typical power of $\sim 2 \times 10^{11}$ W, peak power of roughly an order of magnitude higher and very short duration "S-burst" power up to $\sim 10^{13}$ W at peak [66].

Io acts in its orbit as a moving element in a dynamo, providing an energy source for accelerating electrons and thus powering the Io-DAM CMI. The relative Io-plasma velocity is dominated by the velocity of the rigidly rotating magnetosphere (∼75 km s^{-1} at Io), as that is considerably larger than Io's orbital velocity (∼17.3 km s^{-1}). Io in the Jupiter Io-DAM can thus be treated to a first approximation as a stationary element in a rigidly rotating magnetosphere (which rotates with the rotational period of the planet's deep interior).

In the case of planets or UCDs with rotational CMI, the quasi-rigid rotation of the magnetosphere also seems to be important, and the dynamo effect may be generated in the shear zone where that rigid rotation breaks down [30]. As these objects are much less well understood than the more-accessible solar system CMI emitters, for this paper I will assume that rotational CMI follows the same general scaling relationships as have been derived for unipolar CMI.

Following Vanhamäki [52], the power generated by a satellite orbiting in the magnetosphere can be estimated by

$$P_{unipolar} = \beta \pi R_{moon}^2 \Delta V \frac{\mu_0 \mathcal{M}^2}{32\pi^2 R_{orbital}^6} \text{ W} \tag{15}$$

where R_{moon} is the radius of the Moon as sensed by the magnetosphere (as appropriate, either the solid surface or the top of the atmosphere or magnetosphere), $R_{orbital}$ is the mean radius of the moon's orbit, and ΔV is the difference between the velocity of the magnetosphere and the orbital velocity of the moon. If, as for the Jupiter Io-DAM system, the relative velocity is dominated by the rigid rotation of the magnetosphere, ΔV is $\sim \Omega\ R_{orbital}$, with Ω being the angular rotation frequency of the primary, so that (using Equation 9)

$$P_{unipolar} \propto R_{moon}^2 \frac{M^{2\gamma}\ \Omega^{1+2\varepsilon}}{R_{orbital}^5}\,. \tag{16}$$

$P_{rotational}$ is assumed to follow a similar scaling (without a dependance on R_{moon} of course), with

$$P_{rotational} \propto \frac{M^{2\gamma}\ \Omega^{1+2\varepsilon}}{R_{shear}^5}\,. \tag{17}$$

where R_{shear} is the radius of the shear zone assumed to terminate the magnetospheric currents in rotational CMI.

As a check, the scaling relationships of Equations 15 and 16 can be applied to the Saturnian moon Enceladus, which is a plasma source within Saturn's magnetosphere [67], and thus is a potential source of unipolar CMI radiation. Saturn has about 30% of the mass of Jupiter and Enceladus is at an orbital radius 56% of Io's and has a mean radius only 14% of Io's. The unipolar scaling relation in Equation 16 thus predicts that Enceladus driven unipolar CMI would

only have $\sim 3 \times 10^{-5}$ of the power of the Io-DAM, or $\sim$4 MW, $\sim$0.2% of the total power of the primarily motional Saturn Kilometric Radiation (SKR). The unipolar scaling relation thus predicts that the Saturnian-Enceladus unipolar radio emissions would likely not be separable from the much stronger SKR and in fact it has not yet been observed [68].

There is a large parameter space for unipolar emissions in Equation 15; these parameters are of course unknown for an undiscovered nomadic exoplanet, and, in the complete absence of exomoon data, it is unclear what probability distributions would be appropriate for potential exomoons of hypothetical exoplanets. What is desired is a double power law to scale both $\mathrm{P}_{unipolar}$ and $\mathrm{P}_{motional}$ with the mass and rotational frequency of the primary, when there is, for the mass-power scaling, effectively only a single data point each for both the unipolar and rotational cases. In order to proceed, I estimated a unified double power law by assuming that the peak Io-DAM unipolar power and the UCD burst power are typical emissions for their mass and are both subject to the same scaling with mass and rotation frequency, and also that the rotation frequency exponent ε is the same as for Equation 16, enabling the estimation of the mass scaling from the combination of the Io-DAM and UCD data. As a check of these assumptions, when the rotational scaling exponent $\varepsilon = 0.59$ and Equation 17 are used to adjust for the effects of rotation frequency in the estimates of the radio power for the three UCD sources their spread in power is reduced from a factor of 4.7 to a factor of 1.9, providing some confidence that this scaling applies to rotational as well as unipolar CMI.

Under these assumptions the power generated by unipolar / rotational CMI can be modeled as a triple power law, with

$$P_{unipolar|rotational} \sim P_{Jupiter} \left(\frac{R_{moon}}{R_{Io}}\right)^2 \left(\frac{M}{M_{Jupiter}}\right)^{\zeta} \left(\frac{\Omega}{\Omega_{Jupiter}}\right)^{1+2\varepsilon} \mathrm{W} \ . \tag{18}$$

The mass scaling exponent, ζ, is a free parameter in this model, and was found to be 1.39 ± 0.10 in a least squares solution using the Jupiter and UCD CMI data (of course, the R_{moon} term in Equation 18 should be ignored in estimating

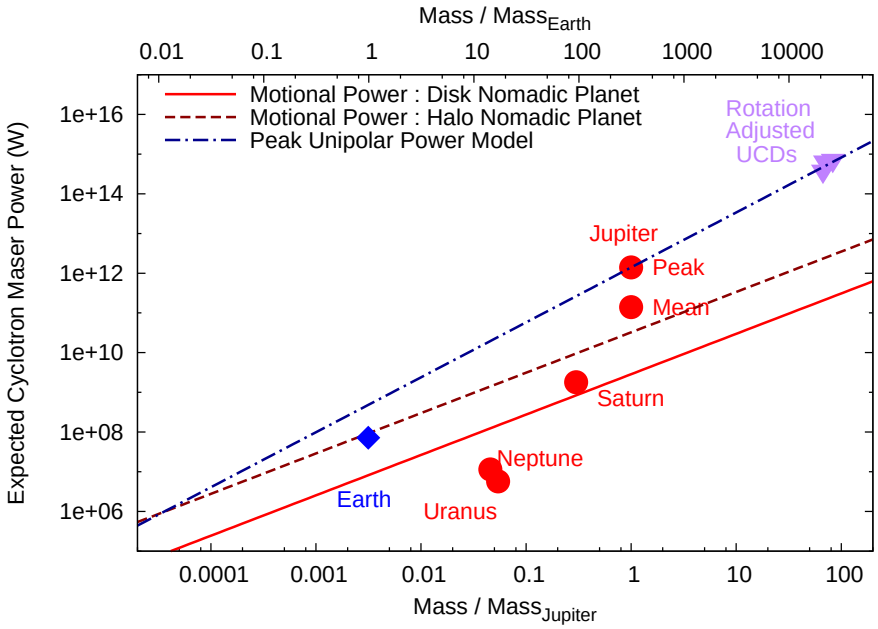

Figure 12: The power generated by various models for ISM radiation by nomadic exoplanets, for motional CMI against the ISM (solid and dashed lines, for a disk and a halo nomad, respectively), together with the unipolar power predicted for an Io-Jupiter analog, respectively, assuming the Jovian rotation period for all masses. The UCD power estimates have been adjusted to the rotation period of Jupiter using the rotation frequency scaling relation of Equation 18

$P_{rotational}$). The model described in Equation 18 is clearly very uncertain, but it does match the very limited available data, and hopefully usefully interpolates the peak power of unipolar and rotational CMI radiation up to ∼80 $M_{Jupiter}$.

6. Searching for Nomadic Planet Radio Emissions

Nomadic planet radio emissions at frequencies above the terrestrial ionospheric low-frequency cutoff will penetrate to the ground and can be observed (if sufficiently bright) by terrestrial radio astronomy. As discussed in subsection 5.1, the peak flux densities from giant planet nomads will likely occur at frequencies between 15–350 MHz, but could extend up almost to 2 GHz for strongly

magnetized exoplanets with masses near the deuterium burning limit. While a number of existing facilities and surveys could potentially detect CMI radiation at relatively high frequencies, new and upgraded radio astronomy facilities sensitive to frequencies at and below 150 MHz are likely to provide the best chanced of detecting the nearby nomadic planets of Jupiter mass and below.

The LOw Frequency ARray (LOFAR) [69], a large new array specifically intended to observe at these relatively low frequencies, is conducting a three-tier sky survey in various channels in the range 15–150 MHz, with "Tier I" being a full survey of the skies visible from Northern Europe, and the Tier II and III surveys consisting of longer integrations restricted to smaller regions of the sky; Table 2 shows the expected sensitivity of these various surveys. The Ukrainian UTR-2 dipole array [49] observes in the frequency range 10-32 MHz and has a sensitivity of ∼10 mJy for a 1 hour integration time, which is a close match to the sensitivity of the LOFAR Tier I survey at 40 MHz. At somewhat higher frequencies, the Indian Giant Metrewave Radio Telescope, or GMRT observes at 150 MHz and is conducting the TIFR survey at that frequency with a median flux density limit of 24.8 mJy [70], and the Murchison Widefield Array in Western Australia can conduct mJy searches for CMI emissions in the Southern sky in the frequency range 80–300 MHz [71, 53].

6.1. Detecting Nomadic Planet CMI Emissions

CMI sources emit radiation in a fairly narrow cone, and can thus only be seen when their emission cone illuminates the observer. This leads to a periodic emission with a fairly small duty cycle (the fraction of time, typically expressed as a percentage, in which a source is active). The UCD sources have duty cycles from 5% to 30%, similar to that of Jupiter's CMI (14%); the rapidly rotating UCDs are thus radio-loud for some minutes or tens of minutes every 2-3 hr while the Io-flux tube is radio-loud for ∼6 hr every 42.5 hr [30]. The existence of a CMI duty cycle, plus the variability of emission strength between cycles, implies that a single short-duration radio observation of a particular region of the sky would not necessarily detect a nearby nomadic planet in that region;

such observations would have to be repeated to reliably detect nomadic planet CMI down to the radio flux density limit.

Figure 12 shows the CMI power estimates from both the motional and unipolar models, together with rough estimates of the cyclotron maser power emitted by the five strongly magnetized planets in the solar system and the three UCD sources; the UCD source powers shown in this Figure have been adjusted to that expected for a planet of the same mass with the rotation rate of Jupiter using the Ω dependance of Equation 18. Two points are shown for Jupiter, corresponding to the mean and peak power; the unipolar model is scaled to fit the peak power. Note that the estimated cyclotron frequency increases rapidly with mass for super-Jupiters (see Figure 11), and thus the total CMI bandwidth is also predicted to increase rapidly with mass for those bodies. As the modeled CMI bandwidth increases faster with mass than does the modeled CMI power, the CMI flux density (which depends on the power per Hz, and thus effectively on the ratio of the power and the cyclotron frequency) is, as is shown in Figures 13–15, predicted to decrease with mass for all three types of CMI emissions for planets with masses larger than Jupiter.

Figures 13 and 14 show the expected motional flux density from the expected nearest nomadic planet as a function of mass, assuming the entire population is comprised of disk (Figure 13) or halo (Figure 14) nomadic planets. The factor of $\sim$10 difference in the relative velocity expected for these populations changes the expected flux densities by a similar factor; while the expected motional CMI flux densities from galactic disk nomads would difficult to detect with the planned full-sky LOFAR surveys, or the UTR-2 or GMRT arrays (Figure 13), the LOFAR Tier I survey at 120 MHz would have a reasonable prospect of detecting motion CMI from nearby halo nomads (Figure 14). Even a failure to detect nomadic planets through motional CMI would bound the number density of halo nomadic planets; of course, if detected, it should be possible to quickly distinguish halo and disk nomads through their proper motions.

Figure 15 shows the expected unipolar/rotational radio flux density as a function of mass for the closest expected nomadic planets based on Equation

Table 2: Estimated "5 σ" flux density limits for the low frequency channels of the three proposed LOFAR surveys, together with the proposed sky coverage for each survey Tier. The UTR-2 telescope survey sensitivity for 10–32 MHz is similar to that of the LOFAR Tier I survey at 40 MHz, while the GMRT TIRF survey at 150 MHz has a mean 5 σ sensitivity of $\sim$25 mJy. The "mass range" in the last column is the range of exoplanet masses that would have emissions in each channel, assuming the "Jupiter-scaling" of cyclotron frequencies (see Figure 11), and a CMI bandwidth of 50% of the cyclotron frequency. These ranges must be regarded as very approximate; for example, Jupiter has an upper CMI cut-off frequency about a factor of 2 higher than that predicted by its dipole moment, and so in reality can be observed at 40 MHz.

Frequency	Tier 1	Tier 2	Tier 3	$\sim$Mass Range
	$\sim 2\ \pi$ sr	$\sim$0.3 sr	$\sim$0.025 sr	"Jupiter-Scaling"
MHz	mJy	mJy	mJy	$M_{Jupiter}$
15	60	-	-	0.4 - 1.3
40	10	3.0	-	1.4 - 3.8
65	5	1.2	-	1.8 - 5.1
120	0.8	0.12	-	2.5 - 7.6
150	-	-	0.035	2.9 - 8.8

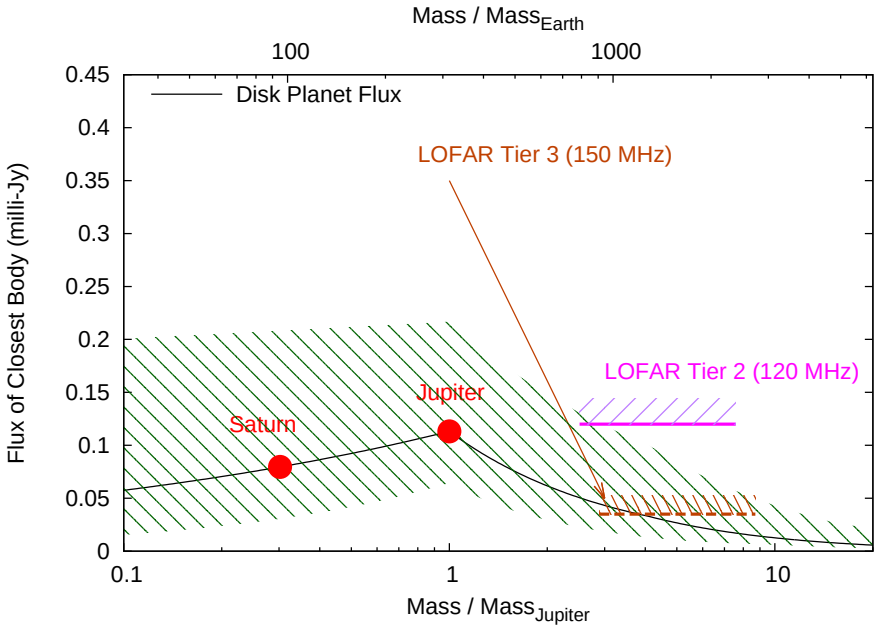

Figure 13: The motional CMI flux density from the expected nearest nomadic planet of a given mass assuming Equations 9 and 14 and a typical relative velocity for the galactic disk nomad, restricted to masses sufficiently large to probably have a cyclotron frequency above the ionospheric cutoff. The LOFAR flux density limits are for the Tier II and Tier III surveys; none of the LOFAR Tier I surveys would have sufficient sensitivity to likely detect motional CMI from a disk nomad. In this and Figures 14 and 15 the survey limits in MHz are expressed in terms of planetary mass assuming a bandwidth of one half the cyclotron frequency and using the formal errors on the Jupiter-scaling of cyclotron frequencies.

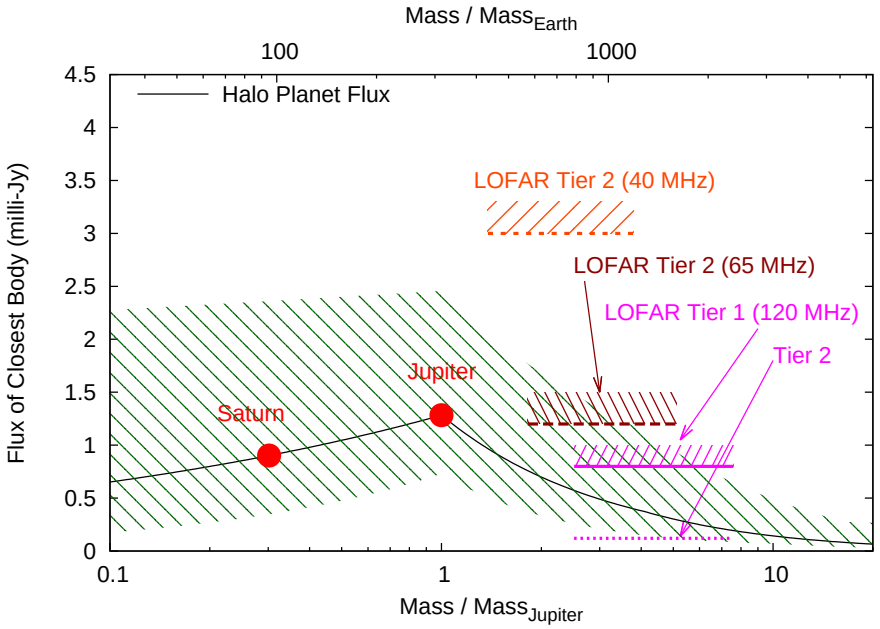

Figure 14: The motional CMI flux density from the expected nearest nomadic planet of a given mass assuming Equations 9 and 14 and a typical relative velocity for a galactic halo object, restricted to masses sufficiently large to probably have a cyclotron frequency above the ionospheric cutoff. The LOFAR flux density limits are for the Tier I and Tier II surveys; the LOFAR Tier I survey at 120 MHz has a good chance of detecting a halo super-Jupiter, assuming that there is a significant population of such objects.

18, together with the various observational limits; the UTR-2 and LOFAR Tier I 40 MHz sensitivities are combined together as they substantially overlap on the scale of this plot. As these various instruments and surveys all have a potential for detecting nomadic CMI emissions, and all cover the full sky observable from their locations, the search for unipolar and rotational CMI emissions probably provides the best ground-based means of discovering nearby nomadic exoplanets, at least for bodies with $M \gtrsim 0.1\ M_{Jupiter}$. (As magnetized exoplanets in stellar systems will be subject to CMI, the search for nomadic radio emissions would also be sensitive to radio-loud Jupiter and super-Jupiters orbiting nearby stars.)

The flux density predictions shown on Figure 15 are based on the assumption that all nomads of a given mass have unipolar or rotational CMI emissions. If, as in the solar system, only one giant planet in four is capable of unipolar CMI emissions, the expected distance to the nearest such nomadic planet would increase by a factor of $4^{1/3}$, and the expected CMI flux density from the nearest radio-loud planet would thus be expected to decrease by a factor of $4^{2/3}$ or $\sim$2.5; this flux density correction is indicated on Figure 15. The UCD flux densities in Figure 15 are adjusted to the expected minimum distance for brown dwarfs, but not for rotation; the fast rotation frequencies of these bodies substantially increases their flux above the model prediction for the rotation period of Jupiter.

If there is a general tendency for exoplanet rotation rates to increase with mass, as is suggested by the rotation rate trend with mass of solar system planets, the $\sim$8.1 hour rotation period of the super-Jupiter β Pictoris b [72], and also by the fast rotating UCDs, nomadic super-Jupiters would be likely to be fast rotators and thus the flux densities predicted in Figure 15 could well be under-estimates. As even with Jupiter's rotation period the peak unipolar flux densities from the closest nomadic super-Jupiters should be detectable with existing instruments, there are thus good prospects of discovering nomadic exoplanet CMI radiation in the 15–350 MHz radio band.

Nomadic planets close enough to have detachable CMI emissions could occur at any galactic latitude and are not likely to show a concentration near the galactic plane. CMI bursts thus potentially could be confused with the still-

mysterious Fast Radio Bursts (FRBs), strongly dispersed radio bursts thought to be from sources at cosmological distances [73, 74], and certainly could be discovered in surveys searching for FRBs (see subsection 6.2). It is even possible that some of the mysterious bursts already detected are due to a nearby exoplanet. Nomadic planet CMI emissions and more exotic extragalactic sources such as the gravitational collapse of neutron stars [75] can be distinguished as the nomadic sources should repeat on some time scale, should lack an optical counterpart, should have significant IR emissions as discussed in Section 4, and, of course, should also have large parallaxes (order 1") and proper motions (order tens of " per year). The most straightforward way of distinguishing CMI bursts and FRBs, however, is likely to be through the different frequency versus time behavior of the bursts : FRBs exhibit an inverse frequency squared dispersion indicating a long journey through the plasma of the InterGalactic Medium (IGM), while CMI bursts have frequency drifts depending on the motion of the emitting region, which will generally have a different frequency dependence with time.

6.2. Advanced Searches for Radio Transients and CMI Radio Emissions

Although Jovian CMI radio emissions have a bandwidth comparable to the cyclotron frequency when averaged over durations long compared to the burst repetition period, the most intense emissions occur in narrow-band, short duration bursts known as S-bursts, which typically have an instantaneous bandwidth of a few kHz shifting in frequency at a median rate of -18 MHz s^{-1}, with a wide range of observed frequency drifts [76, 77]. About 1.5% of the S-bursts actually have positive frequency drifts [76], and a similar fraction exhibit highly perturbed frequency-time patterns, including emission from a single burst being present simultaneously at multiple frequencies [77]. These frequency drifts are thought to be indicative of motion of the radiating region away from the planet (and thus to a lower magnetic field and a lower $f_{cyclotron}$) during the burst [78], possibly combined with the effects of dispersion from the magnetospheric plasma [79]. While less is known about the detailed structure of UCD

CMI bursts, Lynch *et al.* [80], observing the UCDs TVLM 513-46546 and 2M 0746+20 at 5 and 7 GHz, found a somewhat similar burst behavior, with pulse frequency drifts as large as 2 MHz s^{-1} and complicated, time-varying, relations between pulses at different frequencies. From the Jupiter and UCD data, and the physics of CMI emissions, it thus seems likely that exoplanet CMI emissions will predominately occur in bursts with a small instantaneous bandwidth and a time-varying frequency.

A narrow-band receiver following a S-burst frequency shift would see a much higher flux density, possibly 1000 times larger than the time-averaged flux (a rough estimate of the instantaneous narrow-band flux is indicated by the upper dashed line in Figure 15), and also would have a lower receiver Signal to Noise Ratio (SNR). A Jupiter-Io analog at 3.3 ly would, for example, have a peak flux density, averaged over a few minutes, of ∼10 mJy, marginally detectable by either the UTR-2 or the LOFAR Tier I 40 MHz survey. The instantaneous flux of this burst, however, could be could be 1 Jy or stronger over a narrow instantaneous bandwidth (in other words, it could have a fluence > 1 Jy-ms, comparable to the fluences observed with FRB). A matched receiver following such a burst could have a much lower bandwidth, and thus a significantly lower receiver noise, than a conventional wideband receiver, substantially increasing the SNR of burst observations. Searches for nomadic planet CMI emissions would thus benefit from multiple trials of different candidate frequency drifts, a very computationally intensive process requiring in practice either special-purpose hardware or post-observation software processing. Fortunately, the search for highly dispersed pulses and bursts, either from pulsars or from FRBs, also benefits from systematic trials of different pulse dispersion values and there is a long history of such systematic radio searches. It should be possible to broaden the dispersion search algorithms to include the non-dispersive frequency-time behavior of CMI bursts, and thus to integrate the search for nearby exoplanets into ongoing searches for radio pulsars and for FRBs.

Radio waves traversing interstellar and intergalactic space are subject to dispersion by the plasma in the ISM or IGM, which introduces delays propor-

tional to the integrated plasma electron density, the so-called Dispersion Measure (DM), and inversely proportional to the square of the observing frequency, f. (The DM, the integrated free electron content, is generally expressed in units of parsecs cm^{-3}, with 1 pc cm^{-3} $\sim 3 \times 10^{22}$ e^{-} m^{-2}.). A very short-duration pulse of radio waves from a source at galactic or intergalactic distances will be dispersed in frequency, with arrival times as a function of frequency exhibiting an inverse frequency square dependance, with

$$\Delta T_{dispersion}(f) = KDMf^{-2}, \tag{19}$$

where $\Delta_{dispersion}\mathrm{T(f)}$ is the change in arrival time as a function of frequency, and K is a conversion factor. Pulsar and FRB searches thus include a search for a range of DM, and hardware has been developed to facilitate these searches [81, 82, 83].

CMI emissions can vary significantly in amplitude over time and thus could mimic an isolated burst, but will not in general follow the inverse frequency square law of dispersion, and may even have a very irregular change of frequency with time [77]. It appears that, at least for Jupiter, the CMI bursts primarily exhibit linear shifts of frequency with time, so that the change in the arrival time as a function of frequency, $\Delta\mathrm{T}_{CMI}\mathrm{(f)}$, follows

$$\Delta T_{CMI}(f) = Rf, \tag{20}$$

R being the (highly variable, but typically negative) CMI frequency drift rate [76].

It should thus be possible to perform highly sensitive searches for CMI bursts through trials of a wide range of values of R, in much the same way, and for roughly the same computational effort, that searches for FRBs perform trials of a wide range of DM values in their searches for pulses [84]. Even from the available data it is clear that CMI have other differences from FRBs and pulsars (they can, for example, repeat so rapidly that multiple bursts are present simultaneously); the best ways of integrating CMI burst searches and dispersed FRB pulse searches remains a topic for further research.

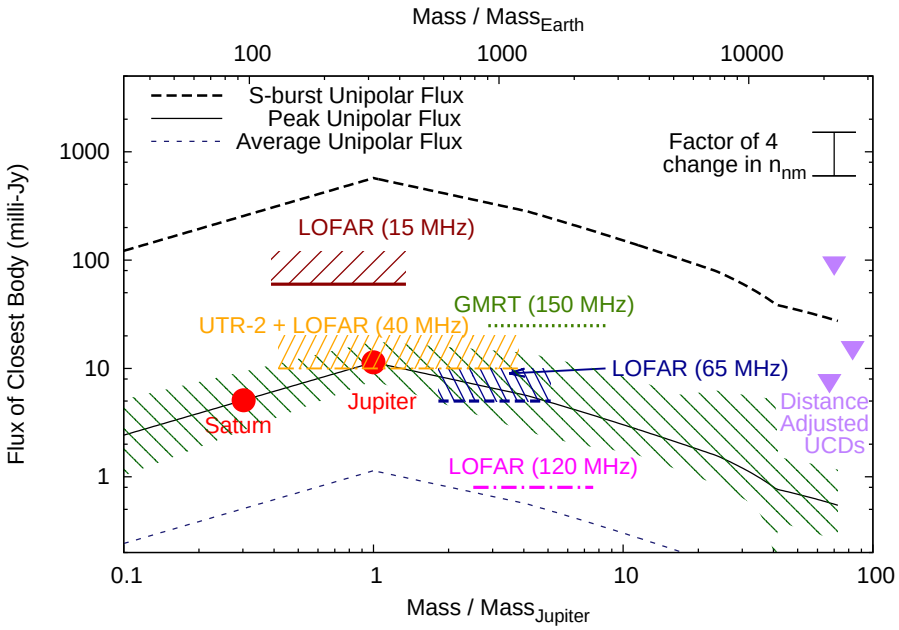

Figure 15: The unipolar flux density from the nearest expected nomadic planet of a given mass assuming Equations 9 and 18 and a rotation period equal to that of Jupiter, together with various LOFAR survey flux density limits and the UTR-2 and GMRT flux density limits. Note that the Jupiter point is based on the actual Jovian unipolar flux density, while the Saturn point is purely based on the model and is included as a convenience for the reader only. The UCD flux densities are adjusted for the difference between the actual UCD distance and the expected minimum distance for a brown dwarf (7.26 ly).

6.3. Electrostatic Discharges from Nearby Nomadic Planets

A potential non-CMI source of non-thermal radio emissions from nearby nomadic exoplanets are emissions caused by electrostatic discharges from planetary lightning. The Voyager and Cassini spacecraft detected lightning-related radio emissions from Saturn, the so-called Saturn Electrostatic Discharges (SED), which have since been observed on the ground by the UTR-2 array [49, 85]. (The radiation from electrostatic discharges on Jupiter is apparently trapped by the Jovian ionosphere, and is not observable from a distance.) The SED are a broad spectrum source up to a limiting frequency of ∼20 MHz, consisting of bursts with a typical duration of order 0.1 s occurring in "episodes" lasting a few hours, with each SED burst having a typical flux density density of order 1 Jy when observed from Earth at a distance of ∼10 AU. While typical SED bursts would have a very small flux density at 2.68 ly (the expected distance for a Saturn mass nomadic exoplanet), the peak SED burst intensity is ∼1000 Jy at 10 AU, equivalent to ∼4 μJy at 2.68 ly, too weak to detect with current surveys, but possibly within reach of a dedicated instrument. Lightning events on Earth can produce X-rays and gamma rays with energies up to ∼2 MeV, and of course also produce visible light, all of which could be conceivably detected across a few light years. If a nearby nomadic exoplanet were to be discovered by other means, electrostatic discharges would be a logical target for follow-up observations; Bailey *et al.*[86] describe various instruments suitable for detecting nearby exoplanet electrostatic discharges across a wide range of energies.

7. Gravitational Lensing of Nearby Nomadic Planets

At present, most exoplanets have been detected either by radial velocity (Doppler) measurements, or by surveys searching for either stellar transits or gravitational microlensing events. While stellar Doppler and orbital transit events are not suitable for detecting nomadic planets, there is some chance of detecting nearby nomadic planets with microlensing. Unfortunately, the optical depths of gravitational lensing of neighboring nomadic planets are sufficiently

low that the detection of significant numbers of nearby nomads by ground based microlensing surveys is unlikely. The integrated optical depth for a lensing event by a single close nomadic planet of $\sim M_{Jupiter}$ would be about 10^{-14} per year, with event duration being of order 1 hour. As there are unlikely to be more than a few hundred Jupiters and super-Jupiters within the detection range of (say) SPICA or JWST (see Table 1), the detection of one such close nomad in a decade would require continual monitoring of order 10^{11} stars. The optical depth is a little more favorable for astrometric mesolensing, with an integrated optical depth of $\sim 3 \times 10^{-12}$ per year for a 20 μas astrometric perturbation of a background star, with such an event lasting on order 2 weeks. As one billion stars is the projected size of the Gaia telescope catalog [87], it is just possible that Gaia would observe such an astrometric mesolensing event over a 5 year mission lifetime [88, 89]. It however seems unlikely that there will be significant numbers of neighboring nomadic planets discovered by microlensing or mesolensing until there are space telescopes dedicated to deep, high-cadence, microlensing or mesolensing surveys.

Neighboring nomadic planets, once discovered, will however be good candidates for predicted microlensing observations [90]. A nearby nomad will be rapidly moving across the sky (a planet at 3.3 ly with a transverse velocity of 30 km s^{-1} would have an angular velocity of $\sim$6 arc sec yr^{-1}); once discovered, it should be possible to search for stars in the future path of such a body and thereby predict and observe upcoming gravitational lensing events, with a goal of directly measuring the planetary mass and detecting or bounding the presence of any companions. Such events have already been predicted, and should be observed, for Proxima Centauri [91], for the same purposes.

For lensing by distant objects (say in the galactic bulge), it is not generally possible to separate the lens and source images, and so for point mass lensing the lens mass, distance and transverse motion are all unknown, leading to degeneracies in the determination of the lens mass. In the case of lensing by a nearby object, the lens distance and transverse velocity can be determined directly from pre and post-event astrometry, and thus a single microlensing event can directly

determine the mass of the lens [91]. A further advantage for predictive nomadic planet lensing is that the lens (the nomadic planet) would have basically no optical emissions and thus would not overwhelm the photometry and astrometry of the background source, as can happen with star-on-star lensing. This would make it possible to observe lensing events with very faint sources, increasing the probability finding an upcoming event. Finally, the Einstein radii of nomadic planet lenses within 5 or 10 ly of the solar system are small enough that in many cases the terrestrial parallax [92] between observatories would be signifiant, and this could also help break lens degeneracies and improve the detectability of lens companions [93].

8. Astrobiology and the Nearby Nomadic Planets

Neighboring nomads will, through planetary migration, provide a sampling of the biological potential (or development) of the galaxy. Terrestrial nomads, either as primaries or as moons of giant nomads, would undoubtedly have very cold exteriors (see Figure 5), but that does not mean that they could not be inhabitable (in an astrobiological sense), potentially supporting active biospheres without being within any stellar habitable zone [94, 95, 96]. Nomad inhabitability would require insulation of a habitable region from the vacuum and heat loss of deep space, and also sources of internal heating, such as by radionuclides or, in the case of exomoons, by tidal heating.

Nomadic planets could thus have "insulated" biospheres evolving under nomadic conditions with no stellar heat input. Stevenson [94] proposed that 1 Earth-mass planets could have surface oceans of liquid water, and thus conceivably biologies, insulated by thick Hydrogen-Helium (H-He) atmospheres with pressure induced far-IR opacity. The subsequent discovery that for $M \gtrsim 4$ M_{Earth} terrestrial planet radii are roughly $\propto$ mass strongly suggests that H-He atmospheres are common for at least these super-Earths [32, 97]; surface water oceans may thus be possible for some super-Earth nomads. Abbot & Switzer [95] have suggested that nomadic "Steppenwolf" planets, with $M \gtrsim 3.5$ M_{Earth},

could have internal liquid water oceans insulated by a thick shell of water (and possibly other) ices. There are of course a number of possible examples in the solar system of insulated internal hydrospheres warmed by tidal heating, with candidates currently including Europa, Callisto, Ganymede, Enceladus, Titan and Triton [98]; there is no reason not to expect similar sub-surface insulated oceans on nomad exomoons [99].

Stellar nomadic planets could also have "fossil" biospheres, the remnants of any biospheres evolving before they were ejected from their stellar system. These could be dead, or the ejected planet biosphere could have subsequently evolved to survive in an insulated ocean, in deep rock formations, or in other insulated regions. These various possibilities thus suggest that the nearest exobiologies could well exist on a yet-to-be-found nearby nomadic planet. It is even possible that nomadic planets ejected sufficiently long after their formation could host remains of technological civilizations. The exploration of nomadic planets thus has the potential of significantly constraining the probability and nature of biologies arising in the galaxy and (should post-formation ejection be common) also the probability of technical civilizations arising in stellar systems in the galaxy.

9. Conclusions

I have shown in this paper that nomadic exoplanets should be found closer than the nearest stars, that these close nomads will sample the galactic history of planetary formation and evolution, and that, while terrestrial nomads will probably be out of reach of the current generation of astronomical instruments, the closest Saturn, Jupiter and super-Jupiter nomads should be discoverable by either their far-IR thermal emission, or by their radio CMI emissions in the 15–350 MHz HF band. Once detected, the neighboring nomadic exoplanets should become a fruitful area of astronomical research; although dim in optical wavelengths, their IR and radio emissions would not be overwhelmed by radiation from a stellar primary, and their closeness would allow detailed astro-

nomical study, for example by the determination of masses through predictive microlensing or by the detection of their electrostatic emissions. Once found, the close nomadic exoplanets should be of astrobiological interest, with a possibility of both fossil biospheres (for planets ejected from stellar systems), and active insulated biospheres (for both ejected and native nomads). In the longer run, as both the closest exoplanets and as possible locations of biospheres, the neighboring nomadic planets are likely to become the initial targets for interstellar exploration by spacecraft.

Acknowledgments

This work was sponsored by Asteroid Initiatives LLC and by Stephanie Eubanks. I am grateful to Bruce Bills and to Adam Crowl for comments and discussions.

References

[1] E. J. Öpik, Stellar Planets and Little Dark Stars as Possible Seats of Life, Irish Astronomical Journal 6 (1964) 290–296.

[2] M. J. Fogg, Interstellar Planets, Comments on Astrophysics 14 (1990) 357.

[3] M. R. Zapatero Osorio, V. J. S. Béjar, E. L. Martín, R. Rebolo, D. Barrado y Navascués, C. A. L. Bailer-Jones, R. Mundt, Discovery of Young, Isolated Planetary Mass Objects in the σ Orionis Star Cluster, Science 290 (2000) 103–107. doi:10.1126/science.290.5489.103.

[4] T. Sumi, K. Kamiya, D. P. Bennett, I. A. Bond, F. Abe, C. S. Botzler, A. Fukui, K. Furusawa, J. B. Hearnshaw, Y. Itow, P. M. Kilmartin, A. Korpela, W. Lin, C. H. Ling, K. Masuda, Y. Matsubara, N. Miyake, M. Motomura, Y. Muraki, M. Nagaya, S. Nakamura, K. Ohnishi, T. Okumura, Y. C. Perrott, N. Rattenbury, T. Saito, T. Sako, D. J. Sullivan, W. L. Sweatman, P. J. Tristram, A. Udalski, M. K. Szymański, M. Kubiak, G. Pietrzyński,

R. Poleski, I. Soszyński, Ł. Wyrzykowski, K. Ulaczyk, Microlensing Observations in Astrophysics (MOA) Collaboration, Unbound or distant planetary mass population detected by gravitational microlensing, Nature 473 (2011) 349–352. arXiv:1105.3544, doi:10.1038/nature10092.

[5] P. Delorme, J. Gagné, L. Malo, C. Reylé, E. Artigau, L. Albert, T. Forveille, X. Delfosse, F. Allard, D. Homeier, CFBDSIR2149-0403: a 4-7 Jupiter-mass free-floating planet in the young moving group AB Doradus?, Astron. Astrophys. 548 (2012) A26. arXiv:1210.0305, doi:10.1051/0004-6361/201219984.

[6] A. W. Howard, G. W. Marcy, D. A. Fischer, H. Isaacson, P. S. Muirhead, G. W. Henry, T. S. Boyajian, K. von Braun, J. C. Becker, J. T. Wright, J. A. Johnson, The NASA-UC-UH ETA-Earth Program. IV. A Low-mass Planet Orbiting an M Dwarf 3.6 PC from Earth, Ap. J. 794 (2014) 51. arXiv:1408.5645, doi:10.1088/0004-637X/794/1/51.

[7] K. L. Luhman, Discovery of a ˜250 K Brown Dwarf at 2 pc from the Sun, Ap. J. Lett. 786 (2014) L18. arXiv:1404.6501, doi:10.1088/2041-8205/786/2/L18.

[8] K. L. Luhman, T. L. Esplin, A New Parallax Measurement for the Coldest Known Brown Dwarf, ArXiv e-printsarXiv:1409.5899.

[9] G. Chabrier, The Galactic Disk Mass Budget. I. Stellar Mass Function and Density, Ap. J. 554 (2001) 1274–1281. arXiv:astro-ph/0107018, doi:10.1086/321401.

[10] R. Roškar, The role of radial migration in shaping the stellar populations of spiral galaxies , Memorie della Societa Astronomica Italiana Supplementi 25 (2013) 64.

[11] D. Veras, A. J. Mustill, A. Bonsor, M. C. Wyatt, Simulations of two-planet systems through all phases of stellar evolution: implications for

the instability boundary and white dwarf pollution, Mon. Not. R.A.S. 431 (2013) 1686–1708. arXiv:1302.3615, doi:10.1093/mnras/stt289.

[12] D. Veras, S. N. Raymond, Planet-planet scattering alone cannot explain the free-floating planet population, Mon. Not. R.A.S. 421 (2012) L117–L121. arXiv:1201.2175, doi:10.1111/j.1745-3933.2012.01218.x.

[13] L. E. Strigari, M. Barnabè, P. J. Marshall, R. D. Blandford, Nomads of the Galaxy, Mon. Not. R.A.S. 423 (2012) 1856–1865. arXiv:1201.2687, doi:10.1111/j.1365-2966.2012.21009.x.

[14] J. D. Kirkpatrick, C. R. Gelino, M. C. Cushing, G. N. Mace, R. L. Griffith, M. F. Skrutskie, K. A. Marsh, E. L. Wright, P. R. Eisenhardt, I. S. McLean, A. K. Mainzer, A. J. Burgasser, C. G. Tinney, S. Parker, G. Salter, Further Defining Spectral Type "Y" and Exploring the Low-mass End of the Field Brown Dwarf Mass Function, Ap. J. 753 (2012) 156. arXiv:1205.2122, doi:10.1088/0004-637X/753/2/156.

[15] J. Bovy, S. Tremaine, On the Local Dark Matter Density, Ap. J. 756 (2012) 89. arXiv:1205.4033, doi:10.1088/0004-637X/756/1/89.

[16] C. Alcock, R. A. Allsman, D. Alves, R. Ansari, E. Aubourg, T. S. Axelrod, P. Bareyre, J.-P. Beaulieu, A. C. Becker, D. P. Bennett, S. Brehin, F. Cavalier, S. Char, K. H. Cook, R. Ferlet, J. Fernandez, K. C. Freeman, K. Griest, P. Grison, M. Gros, C. Gry, J. Guibert, M. Lachieze-Rey, B. Laurent, M. J. Lehner, E. Lesquoy, C. Magneville, S. L. Marshall, E. Maurice, A. Milsztajn, D. Minniti, M. Moniez, O. Moreau, L. Moscoso, N. Palanque-Delabrouille, B. A. Peterson, M. R. Pratt, L. Prevot, F. Queinnec, P. J. Quinn, C. Renault, J. Rich, M. Spiro, C. W. Stubbs, W. Sutherland, A. Tomaney, T. Vandehei, A. Vidal-Madjar, L. Vigroux, S. Zylberajch, EROS and MACHO Combined Limits on Planetary-Mass Dark Matter in the Galactic Halo, Ap. J. Lett. 499 (1998) L9.

[17] J. J. Lissauer, R. I. Dawson, S. Tremaine, Advances in exoplanet

science from Kepler, Nature 513 (2014) 336–344. arXiv:1409.1595, doi:10.1038/nature13781.

[18] M. Mayor, C. Lovis, N. C. Santos, Doppler spectroscopy as a path to the detection of Earth-like planets, Nature 513 (2014) 328–335. doi:10.1038/nature13780.

[19] K. L. Luhman, A Search for a Distant Companion to the Sun with the Wide-field Infrared Survey Explorer, Ap. J. 781 (2014) 4. doi:10.1088/0004-637X/781/1/4.

[20] K. L. Luhman, Discovery of a Binary Brown Dwarf at 2 pc from the Sun, Ap. J. Lett. 767 (2013) L1. arXiv:1303.2401, doi:10.1088/2041-8205/767/1/L1.

[21] K. Griest, A. M. Cieplak, M. J. Lehner, New Limits on Primordial Black Hole Dark Matter from an Analysis of Kepler Source Microlensing Data, Phys. Rev. Lett. 111 (18) (2013) 181302. doi:10.1103/PhysRevLett.111.181302.

[22] A. M. Cieplak, K. Griest, Improved Theoretical Predictions of Microlensing Rates for the Detection of Primordial Black Hole Dark Matter, Ap. J. 767 (2013) 145. arXiv:1210.7729, doi:10.1088/0004-637X/767/2/145.

[23] Y. K. Jung, H. Park, C. Han, K.-H. Hwang, I.-G. Shin, J.-Y. Choi, Reevaluating the Feasibility of Ground-based Earth-mass Microlensing Planet Detections, Ap. J. 786 (2014) 85. arXiv:1403.1032, doi:10.1088/0004-637X/786/2/85.

[24] J.-P. Beaulieu, P. Tisserand, V. Batista, Space based microlensing planet searches, in: European Physical Journal Web of Conferences, Vol. 47 of European Physical Journal Web of Conferences, 2013, p. 15001. arXiv:1303.6783, doi:10.1051/epjconf/20134715001.

[25] E. F. del Peloso, L. da Silva, G. F. Porto de Mello, L. I. Arany-Prado, The age of the Galactic thin disk from Th/Eu nucleocosmochronol-

ogy. III. Extended sample, Astron. Astrophys. 440 (2005) 1153–1159. arXiv:astro-ph/0506458, doi:10.1051/0004-6361:20053307.

[26] L. Vican, Age Determination for 346 Nearby Stars in the Herschel DEBRIS Survey, Astron. J. 143 (2012) 135. arXiv:1203.1966, doi:10.1088/0004-6256/143/6/135.

[27] J. J. Fortney, M. Ikoma, N. Nettelmann, T. Guillot, M. S. Marley, Self-consistent Model Atmospheres and the Cooling of the Solar System's Giant Planets, Ap. J. 729 (2011) 32. arXiv:1101.0606, doi:10.1088/0004-637X/729/1/32.

[28] E. A. Frank, B. S. Meyer, S. J. Mojzsis, A radiogenic heating evolution model for cosmochemically Earth-like exoplanets, Icarus 243 (2014) 274–286. doi:10.1016/j.icarus.2014.08.031.

[29] J. Schneider, C. Dedieu, P. Le Sidaner, R. Savalle, I. Zolotukhin, Defining and cataloging exoplanets: the exoplanet.eu database, Astron. Astrophys. 532 (2011) A79. arXiv:1106.0586, doi:10.1051/0004-6361/201116713.

[30] J. D. Nichols, M. R. Burleigh, S. L. Casewell, S. W. H. Cowley, G. A. Wynn, J. T. Clarke, A. A. West, Origin of Electron Cyclotron Maser Induced Radio Emissions at Ultracool Dwarfs: Magnetosphere-Ionosphere Coupling Currents, Ap. J. 760 (2012) 59. arXiv:1210.1864, doi:10.1088/0004-637X/760/1/59.

[31] G. Chabrier, I. Baraffe, J. Leconte, J. Gallardo, T. Barman, The mass-radius relationship from solar-type stars to terrestrial planets: a review, in: E. Stempels (Ed.), 15th Cambridge Workshop on Cool Stars, Stellar Systems, and the Sun, Vol. 1094 of American Institute of Physics Conference Series, 2009, pp. 102–111. arXiv:0810.5085, doi:10.1063/1.3099078.

[32] G. W. Marcy, L. M. Weiss, E. A. Petigura, H. Isaacson, A. W. Howard, L. A. Buchhave, Occurrence and core-envelope structure of 1–4x Earth-size planets around Sun-like stars, ArXiv e-printsarXiv:1404.2960.

[33] N. Haghighipour, Super-Earths: a new class of planetary bodies, Contemporary Physics 52 (2011) 403–438. arXiv:1108.0031, doi:10.1080/00107514.2011.598370.

[34] C. Mordasini, Y. Alibert, C. Georgy, K.-M. Dittkrist, H. Klahr, T. Henning, Characterization of exoplanets from their formation. II. The planetary mass-radius relationship, Astron. Astrophys. 547 (2012) A112. arXiv:1206.3303, doi:10.1051/0004-6361/201118464.

[35] A. P. Hatzes, The role of space telescopes in the characterization of transiting exoplanets, Nature 513 (2014) 353–357. doi:10.1038/nature13783.

[36] J. H. Davies, D. R. Davies, Earth's surface heat flux, Solid Earth 1 (1) (2010) 5–24. doi:10.5194/se-1-5-2010.
URL http://www.solid-earth.net/1/5/2010/

[37] M. A. Siegler, S. E. Smrekar, Lunar heat flow: Regional prospective of the Apollo landing sites, J. Geophys. Res. (Planets) 119 (2014) 47–63. doi:10.1002/2013JE004453.

[38] L. Li, K. H. Baines, M. A. Smith, R. A. West, S. Pérez-Hoyos, H. J. Trammell, A. A. Simon-Miller, B. J. Conrath, P. J. Gierasch, G. S. Orton, C. A. Nixon, G. Filacchione, P. M. Fry, T. W. Momary, Emitted power of Jupiter based on Cassini CIRS and VIMS observations, J. Geophys. Res. (Planets) 117 (E16) (2012) 11002. doi:10.1029/2012JE004191.

[39] R. A. Hanel, B. J. Conrath, V. G. Kunde, J. C. Pearl, J. A. Pirraglia, Albedo, internal heat flux, and energy balance of Saturn, Icarus 53 (1983) 262–285. doi:10.1016/0019-1035(83)90147-1.

[40] L. Li, B. J. Conrath, P. J. Gierasch, R. K. Achterberg, C. A. Nixon, A. A. Simon-Miller, F. M. Flasar, D. Banfield, K. H. Baines, R. A. West, A. P. Ingersoll, A. R. Vasavada, A. D. Del Genio, C. C. Porco, A. A. Mamoutkine, M. E. Segura, G. L. Bjoraker, G. S. Orton, L. N. Fletcher, P. G. J. Irwin,

P. L. Read, Saturn's emitted power, J. Geophys. Res. (Planets) 115 (E14) (2010) 11002. doi:10.1029/2010JE003631.

[41] M. T. Stier, W. A. Traub, E. L. Wright, F. J. Low, Far-infrared observations of Uranus, Neptune, and Ceres, Ap. J. 226 (1978) 347–349. doi:10.1086/156614.

[42] J. C. Pearl, B. J. Conrath, R. A. Hanel, J. A. Pirraglia, The albedo, effective temperature, and energy balance of Uranus, as determined from Voyager IRIS data, Icarus 84 (1990) 12–28. doi:10.1016/0019-1035(90)90155-3.

[43] J. C. Pearl, B. J. Conrath, The albedo, effective temperature, and energy balance of Neptune, as determined from Voyager data, J. Geophys. Res. 96 (1991) 18921.

[44] A. Baudry, The ALMA radio telescope, in: 2nd MCCT-SKADS Training School. Radio Astronomy: Fundamentals and the New Instruments, 2008.

[45] E. L. Wright, P. R. M. Eisenhardt, A. K. Mainzer, M. E. Ressler, R. M. Cutri, T. Jarrett, J. D. Kirkpatrick, D. Padgett, R. S. McMillan, M. Skrutskie, S. A. Stanford, M. Cohen, R. G. Walker, J. C. Mather, D. Leisawitz, T. N. Gautier, III, I. McLean, D. Benford, C. J. Lonsdale, A. Blain, B. Mendez, W. R. Irace, V. Duval, F. Liu, D. Royer, I. Heinrichsen, J. Howard, M. Shannon, M. Kendall, A. L. Walsh, M. Larsen, J. G. Cardon, S. Schick, M. Schwalm, M. Abid, B. Fabinsky, L. Naes, C.-W. Tsai, The Wide-field Infrared Survey Explorer (WISE): Mission Description and Initial On-orbit Performance, Astron. J. 140 (2010) 1868–1881. arXiv:1008.0031, doi:10.1088/0004-6256/140/6/1868.

[46] M. J. Barlow, The impact of future space observatories on planetary nebula research, in: IAU Symposium, Vol. 283 of IAU Symposium, 2012, pp. 295–301. doi:10.1017/S174392131201112X.

[47] T. Onaka, T. Nakagawa, T. Matsumoto, H. Murakami, H. Matsuhara, H. Kataza, H. Kaneda, K. Enya, Y. Y. Yui, M. Tamura, Telescope system

of the Space Infrared Telescope for Cosmology and Astrophysics (SPICA) mission, in: B. Warmbein (Ed.), 5th International Conference on Space Optics, Vol. 554 of ESA Special Publication, 2004, pp. 297–302.

[48] P. Zarka, Auroral radio emissions at the outer planets: Observations and theories, J. Geophys. Res. 103 (1998) 20159–20194. doi:10.1029/98JE01323.

[49] J.-M. Grießmeier, P. Zarka, J. N. Girard, Observation of planetary radio emissions using large arrays, Radio Science 46 (2011) 0. doi:10.1029/2011RS004752.

[50] B. Cecconi, S. Hess, A. Hérique, M. R. Santovito, D. Santos-Costa, P. Zarka, G. Alberti, D. Blankenship, J.-L. Bougeret, L. Bruzzone, W. Kofman, Natural radio emission of Jupiter as interferences for radar investigations of the icy satellites of Jupiter, Planet. Space Sci. 61 (2012) 32–45. doi:10.1016/j.pss.2011.06.012.

[51] T. J. Lazio, W., W. M. Farrell, J. Dietrick, E. Greenlees, E. Hogan, C. Jones, L. A. Hennig, The Radiometric Bode's Law and Extrasolar Planets, Ap. J. 612 (2004) 511–518. doi:10.1086/422449.

[52] H. Vanhamäki, Emission of cyclotron radiation by interstellar planets, Planet. Space Sci. 59 (2011) 862–869. doi:10.1016/j.pss.2011.04.002.

[53] T. Murphy, M. E. Bell, D. L. Kaplan, B. M. Gaensler, A. R. Offringa, E. Lenc, N. Hurley-Walker, G. Bernardi, J. D. Bowman, F. Briggs, R. J. Cappallo, B. E. Corey, A. A. Deshpande, D. Emrich, R. Goeke, L. J. Greenhill, B. J. Hazelton, J. N. Hewitt, M. Johnston-Hollitt, J. C. Kasper, E. Kratzenberg, C. J. Lonsdale, M. J. Lynch, S. R. McWhirter, D. A. Mitchell, M. F. Morales, E. Morgan, D. Oberoi, S. M. Ord, T. Prabu, A. E. E. Rogers, D. A. Roshi, N. Udaya Shankar, K. S. Srivani, R. Subrahmanyan, S. J. Tingay, M. Waterson, R. B. Wayth, R. L. Webster, A. R.

Whitney, A. Williams, C. L. Williams, Limits on low frequency radio emission from southern exoplanets with the Murchison Widefield Array, ArXiv e-printsarXiv:1410.6819.

[54] M. Route, A. Wolszczan, The 5 GHz Arecibo Search for Radio Flares from Ultracool Dwarfs, Ap. J. 773 (2013) 18. arXiv:1306.1152, doi:10.1088/0004-637X/773/1/18.

[55] G. Hallinan, A. Antonova, J. G. Doyle, S. Bourke, C. Lane, A. Golden, Confirmation of the Electron Cyclotron Maser Instability as the Dominant Source of Radio Emission from Very Low Mass Stars and Brown Dwarfs, Ap. J. 684 (2008) 644–653. arXiv:0805.4010, doi:10.1086/590360.

[56] J. Forbrich, S. J. Wolk, M. Güdel, A. Benz, R. Osten, J. L. Linsky, M. McLean, L. Loinard, E. Berger, The Radio-X-ray Relation in Cool Stars: Are We Headed Toward a Divorce?, in: C. Johns-Krull, M. K. Browning, A. A. West (Eds.), 16th Cambridge Workshop on Cool Stars, Stellar Systems, and the Sun, Vol. 448 of Astronomical Society of the Pacific Conference Series, 2011, p. 455. arXiv:1012.1626.

[57] H. J. Durand-Manterola, Dipolar magnetic moment of the bodies of the solar system and the Hot Jupiters, Planetary and Space Science 57 (2009) 1405–1411. doi:10.1016/j.pss.2009.06.024.

[58] A. Ekenbäck, M. Holmström, P. Wurz, J.-M. Grießmeier, H. Lammer, F. Selsis, T. Penz, Energetic Neutral Atoms Around HD 209458b: Estimations of Magnetospheric Properties, Ap. J. 709 (2010) 670–679. doi:10.1088/0004-637X/709/2/670.

[59] K. G. Kislyakova1, M. Holmstrm, H. Lammer, P. Odert, M. L. Khodachenko, Magnetic moment and plasma environment of HD 209458b as determined from Lyα observations, Science 346 (2014) 981–984. doi:10.1126/science.1257829.

[60] E. Rauscher, E. M. R. Kempton, The Atmospheric Circulation and Observable Properties of Non-synchronously Rotating Hot Jupiters, Ap. J. 790 (2014) 79. arXiv:1402.4833, doi:10.1088/0004-637X/790/1/79.

[61] J. G. Doyle, A. Antonova, M. S. Marsh, G. Hallinan, S. Yu, A. Golden, Phase connecting multi-epoch radio data for the ultracool dwarf TVLM 513-46546, Astron. Astrophys. 524 (2010) A15. doi:10.1051/0004-6361/201015274.

[62] A. Lecavelier Des Etangs, S. K. Sirothia, Gopal-Krishna, P. Zarka, GMRT search for 150 MHz radio emission from the transiting extrasolar planets HD 189733 b and HD 209458 b, Astron. Astrophys. 533 (2011) A50. arXiv:1108.3730, doi:10.1051/0004-6361/201117330.

[63] S. Jester, H. Falcke, Science with a lunar low-frequency array: From the dark ages of the Universe to nearby exoplanets, New Astronomy Reviews 53 (2009) 1–26. arXiv:0902.0493, doi:10.1016/j.newar.2009.02.001.

[64] F. Nesti, P. Salucci, The Dark Matter Halo of the Milky Way, AD 2013, J. Cosmology and Astroparticle Physics 7 (2013) 16. arXiv:1304.5127, doi:10.1088/1475-7516/2013/07/016.

[65] P. Zarka, Radioastronomy and the Study of Exoplanets, in: V. Coudé du Foresto, D. M. Gelino, I. Ribas (Eds.), Pathways Towards Habitable Planets, Vol. 430 of Astronomical Society of the Pacific Conference Series, 2010, p. 175.

[66] S. K. Bose, S. Sarkar, A. B. Bhattacharyya, Jovian decametric radio emissions: An overview of the planetary radio astronomical observations, Indian Journal of Radio and Space Physics 37 (2008) 77–108.

[67] D. H. Pontius, T. W. Hill, Enceladus: A significant plasma source for Saturn's magnetosphere, Journal of Geophysical Research (Space Physics) 111 (2006) 9214. doi:10.1029/2006JA011674.

[68] J. D. Menietti, J. B. Groene, T. F. Averkamp, G. B. Hospodarsky, W. S. Kurth, D. A. Gurnett, P. Zarka, Influence of Saturnian moons on Saturn kilometric radiation, Journal of Geophysical Research (Space Physics) 112 (2007) 8211. doi:10.1029/2007JA012331.

[69] M. P. van Haarlem, M. W. Wise, A. W. Gunst, G. Heald, J. P. McKean, J. W. T. Hessels, A. G. de Bruyn, R. Nijboer, J. Swinbank, R. Fallows, M. Brentjens, A. Nelles, R. Beck, H. Falcke, R. Fender, J. Hörandel, L. V. E. Koopmans, G. Mann, G. Miley, H. Röttgering, B. W. Stappers, R. A. M. J. Wijers, S. Zaroubi, M. van den Akker, A. Alexov, J. Anderson, K. Anderson, A. van Ardenne, M. Arts, A. Asgekar, I. M. Avruch, F. Batejat, L. Bähren, M. E. Bell, M. R. Bell, I. van Bemmel, P. Bennema, M. J. Bentum, G. Bernardi, P. Best, L. Bîrzan, A. Bonafede, A.-J. Boonstra, R. Braun, J. Bregman, F. Breitling, R. H. van de Brink, J. Broderick, P. C. Broekema, W. N. Brouw, M. Brüggen, H. R. Butcher, W. van Cappellen, B. Ciardi, T. Coenen, J. Conway, A. Coolen, A. Corstanje, S. Damstra, O. Davies, A. T. Deller, R.-J. Dettmar, G. van Diepen, K. Dijkstra, P. Donker, A. Doorduin, J. Dromer, M. Drost, A. van Duin, J. Eislöffel, J. van Enst, C. Ferrari, W. Frieswijk, H. Gankema, M. A. Garrett, F. de Gasperin, M. Gerbers, E. de Geus, J.-M. Grießmeier, T. Grit, P. Gruppen, J. P. Hamaker, T. Hassall, M. Hoeft, H. A. Holties, A. Horneffer, A. van der Horst, A. van Houwelingen, A. Huijgen, M. Iacobelli, H. Intema, N. Jackson, V. Jelic, A. de Jong, E. Juette, D. Kant, A. Karastergiou, A. Koers, H. Kollen, V. I. Kondratiev, E. Kooistra, Y. Koopman, A. Koster, M. Kuniyoshi, M. Kramer, G. Kuper, P. Lambropoulos, C. Law, J. van Leeuwen, J. Lemaitre, M. Loose, P. Maat, G. Macario, S. Markoff, J. Masters, R. A. McFadden, D. McKay-Bukowski, H. Meijering, H. Meulman, M. Mevius, E. Middelberg, R. Millenaar, J. C. A. Miller-Jones, R. N. Mohan, J. D. Mol, J. Morawietz, R. Morganti, D. D. Mulcahy, E. Mulder, H. Munk, L. Nieuwenhuis, R. van Nieuwpoort, J. E. Noordam, M. Norden, A. Noutsos, A. R. Offringa, H. Olofsson, A. Omar, E. Orrú, R. Overeem,

H. Paas, M. Pandey-Pommier, V. N. Pandey, R. Pizzo, A. Polatidis, D. Rafferty, S. Rawlings, W. Reich, J.-P. de Reijer, J. Reitsma, G. A. Renting, P. Riemers, E. Rol, J. W. Romein, J. Roosjen, M. Ruiter, A. Scaife, K. van der Schaaf, B. Scheers, P. Schellart, A. Schoenmakers, G. Schoonderbeek, M. Serylak, A. Shulevski, J. Sluman, O. Smirnov, C. Sobey, H. Spreeuw, M. Steinmetz, C. G. M. Sterks, H.-J. Stiepel, K. Stuurwold, M. Tagger, Y. Tang, C. Tasse, I. Thomas, S. Thoudam, M. C. Toribio, B. van der Tol, O. Usov, M. van Veelen, A.-J. van der Veen, S. ter Veen, J. P. W. Verbiest, R. Vermeulen, N. Vermaas, C. Vocks, C. Vogt, M. de Vos, E. van der Wal, R. van Weeren, H. Weggemans, P. Weltevrede, S. White, S. J. Wijnholds, T. Wilhelmsson, O. Wucknitz, S. Yatawatta, P. Zarka, A. Zensus, J. van Zwieten, LOFAR: The LOw-Frequency ARray, Astron. Astrophys. 556 (2013) A2. arXiv:1305.3550, doi:10.1051/0004-6361/201220873.

[70] S. K. Sirothia, A. Lecavelier des Etangs, Gopal-Krishna, N. G. Kantharia, C. H. Ishwar-Chandra, Search for 150 MHz radio emission from extrasolar planets in the TIFR GMRT Sky Survey, Astron. Astrophys. 562 (2014) A108. doi:10.1051/0004-6361/201321571.

[71] C. J. Lonsdale, R. J. Cappallo, M. F. Morales, F. H. Briggs, L. Benkevitch, J. D. Bowman, J. D. Bunton, S. Burns, B. E. Corey, L. Desouza, S. S. Doeleman, M. Derome, A. Deshpande, M. R. Gopala, L. J. Greenhill, D. E. Herne, J. N. Hewitt, P. A. Kamini, J. C. Kasper, B. B. Kincaid, J. Kocz, E. Kowald, E. Kratzenberg, D. Kumar, M. J. Lynch, S. Madhavi, M. Matejek, D. A. Mitchell, E. Morgan, D. Oberoi, S. Ord, J. Pathikulangara, T. Prabu, A. Rogers, A. Roshi, J. E. Salah, R. J. Sault, N. U. Shankar, K. S. Srivani, J. Stevens, S. Tingay, A. Vaccarella, M. Waterson, R. B. Wayth, R. L. Webster, A. R. Whitney, A. Williams, C. Williams, The Murchison Widefield Array: Design Overview, IEEE Proceedings 97 (2009) 1497–1506. arXiv:0903.1828, doi:10.1109/JPROC.2009.2017564.

[72] I. A. G. Snellen, B. R. Brandl, R. J. de Kok, M. Brogi, J. Birkby,

H. Schwarz, Fast spin of the young extrasolar planet β Pictoris b, Nature 509 (2014) 63–65. doi:10.1038/nature13253.

[73] D. R. Lorimer, M. Bailes, M. A. McLaughlin, D. J. Narkevic, F. Crawford, A Bright Millisecond Radio Burst of Extragalactic Origin, Science 318 (2007) 777–. arXiv:0709.4301, doi:10.1126/science.1147532.

[74] D. Thornton, B. Stappers, M. Bailes, B. Barsdell, S. Bates, N. D. R. Bhat, M. Burgay, S. Burke-Spolaor, D. J. Champion, P. Coster, N. D'Amico, A. Jameson, S. Johnston, M. Keith, M. Kramer, L. Levin, S. Milia, C. Ng, A. Possenti, W. van Straten, A Population of Fast Radio Bursts at Cosmological Distances, Science 341 (2013) 53–56. arXiv:1307.1628, doi:10.1126/science.1236789.

[75] J. Fuller, C. Ott, Dark Matter-induced Collapse of Neutron Stars: A Possible Link Between Fast Radio Bursts and the Missing Pulsar Problem, ArXiv e-printsarXiv:1412.6119.

[76] P. Zarka, T. Farges, B. P. Ryabov, M. Abada-Simon, L. Denis, A scenario for Jovian S-bursts, Geophys. Res. Lett. 23 (1996) 125–128. doi:10.1029/95GL03780.

[77] V. B. Ryabov, B. P. Ryabov, D. M. Vavriv, P. Zarka, R. Kozhin, V. V. Vinogradov, V. A. Shevchenko, Jupiter S-bursts: Narrow-band origin of microsecond subpulses, J. Geophys. Res. (Space Physics) 112 (2007) 9206. doi:10.1029/2007JA012607.

[78] S. Hess, B. Cecconi, P. Zarka, Modeling of Io-Jupiter decameter arcs, emission beaming and energy source, Geophys. Res. Lett. 35 (2008) L13107. doi:10.1029/2008GL033656.

[79] O. V. Arkhypov, H. O. Rucker, Dispersion-like phenomena in Jovian decametric S-bursts: Tabooed Facts, ArXiv e-printsarXiv:1402.1966.

[80] C. Lynch, R. L. Mutel, M. Gudel, Wideband Dynamic Radio Spectra of Two Ultra-cool dwarfs, ArXiv e-printsarXiv:1405.3516.

[81] A. Magro, A. Karastergiou, S. Salvini, B. Mort, F. Dulwich, K. Zarb Adami, Real-time, fast radio transient searches with GPU dedispersion, Mon. Not. R.A.S. 417 (2011) 2642–2650. arXiv:1107.2516, doi:10.1111/j.1365-2966.2011.19426.x.

[82] B. R. Barsdell, M. Bailes, D. G. Barnes, C. J. Fluke, Spotting Radio Transients with the Help of GPUs, in: P. Ballester, D. Egret, N. P. F. Lorente (Eds.), Astronomical Data Analysis Software and Systems XXI, Vol. 461 of Astronomical Society of the Pacific Conference Series, 2012, p. 37. arXiv:1112.0065.

[83] N. Clarke, L. D'Addario, R. Navarro, J. Trinh, A Multi-Beam Radio Transient Detector with Real-Time De-Dispersion Over a Wide DM Range, Journal of Astronomical Instrumentation 3 (2014) 50004. arXiv:1403.2468, doi:10.1142/S2251171714500044.

[84] C. J. Law, G. C. Bower, S. Burke-Spolaor, B. Butler, E. Lawrence, T. J. W. Lazio, C. A. Mattmann, M. Rupen, A. Siemion, S. VanderWiel, A Millisecond Interferometric Search for Fast Radio Bursts with the Very Large Array, ArXiv e-printsarXiv:1412.7536.

[85] J.-M. Grießmeier, P. Zarka, A. Konovalenko, G. Fischer, V. Zakharenko, B. W. Stappers, J. N. Girard, B. Ryabov, D. Vavriv, V. Ryabov, H. O. Rucker, Ground-Based Study of Saturn Lightning, Planetary, Solar and Heliospheric Radio Emissions (PRE VII) (2011) 145–154.

[86] R. L. Bailey, C. Helling, G. Hodosán, C. Bilger, C. R. Stark, Ionization in Atmospheres of Brown Dwarfs and Extrasolar Planets VI: Properties of Large-scale Discharge Events, Ap. J. 784 (2014) 43. arXiv:1312.6789, doi:10.1088/0004-637X/784/1/43.

[87] L. Lindegren, Gaia: Astrometric performance and current status of the project, in: S. A. Klioner, P. K. Seidelmann, M. H. Soffel (Eds.), IAU Symposium, Vol. 261 of IAU Symposium, 2010, pp. 296–305. doi:10.1017/S1743921309990548.

[88] V. A. Belokurov, N. W. Evans, Astrometric microlensing with the GAIA satellite, Mon. Not. R.A.S. 331 (2002) 649–665. arXiv:astro-ph/0112243, doi:10.1046/j.1365-8711.2002.05222.x.

[89] B. S. Gaudi, J. S. Bloom, Astrometric Microlensing Constraints on a Massive Body in the Outer Solar System with Gaia, Ap. J. 635 (2005) 711–717. arXiv:astro-ph/0506426, doi:10.1086/497391.

[90] B. Paczynski, The Masses of Nearby Dwarfs Can Be Determined with Gravitational Microlensing, Acta Astronomica 45 (1995) 345–348. arXiv:astro-ph/9504099.

[91] K. C. Sahu, H. E. Bond, J. Anderson, M. Dominik, Microlensing Events by Proxima Centauri in 2014 and 2016: Opportunities for Mass Determination and Possible Planet Detection, Ap. J. 782 (2014) 89. arXiv:1401.0239, doi:10.1088/0004-637X/782/2/89.

[92] A. Gould, A. Udalski, B. Monard, K. Horne, S. Dong, N. Miyake, K. Sahu, D. P. Bennett, Ł. Wyrzykowski, I. Soszyński, M. K. Szymański, M. Kubiak, G. Pietrzyński, O. Szewczyk, K. Ulaczyk, OGLE Collaboration, W. Allen, G. W. Christie, D. L. DePoy, B. S. Gaudi, C. Han, C.-U. Lee, J. McCormick, T. Natusch, B.-G. Park, R. W. Pogge, μFUN Collaboration, A. Allan, M. F. Bode, D. M. Bramich, M. J. Burgdorf, M. Dominik, S. N. Fraser, E. Kerins, C. Mottram, C. Snodgrass, I. A. Steele, R. Street, Y. Tsapras, RoboNet Collaboration, F. Abe, I. A. Bond, C. S. Botzler, A. Fukui, K. Furusawa, J. B. Hearnshaw, Y. Itow, K. Kamiya, P. M. Kilmartin, A. Korpela, W. Lin, C. H. Ling, K. Masuda, Y. Matsubara, Y. Muraki, M. Nagaya, K. Ohnishi, T. Okumura, Y. C. Perrott, N. Rattenbury, T. Saito, T. Sako, L. Skuljan, D. J. Sullivan, T. Sumi, W. L. Sweatman, P. J. Tristram, P. C. M. Yock, MOA Collaboration, M. Albrow, J. P. Beaulieu, C. Coutures, H. Calitz, J. Caldwell, P. Fouque, R. Martin, A. Williams, PLANET Collaboration, The Extreme Microlensing Event OGLE-2007-BLG-224: Terrestrial Par-

allax Observation of a Thick-Disk Brown Dwarf, Ap. J. Lett. 698 (2009) L147–L151. arXiv:0904.0249, doi:10.1088/0004-637X/698/2/L147.

[93] A. Gould, J. C. Yee, Microlens Terrestrial Parallax Mass Measurements: A Rare Probe of Isolated Brown Dwarfs and Free-floating Planets, Ap. J. 764 (2013) 107. arXiv:1212.1732, doi:10.1088/0004-637X/764/1/107.

[94] D. J. Stevenson, Life-sustaining planets in interstellar space?, Nature 400 (1999) 32. doi:10.1038/21811.

[95] D. S. Abbot, E. R. Switzer, The Steppenwolf: A Proposal for a Habitable Planet in Interstellar Space, Ap. J. Lett. 735 (2011) L27. arXiv:1102.1108, doi:10.1088/2041-8205/735/2/L27.

[96] V. Badescu, Free-floating planets as potential seats for aqueous and non-aqueous life, Icarus 216 (2011) 485–491. doi:10.1016/j.icarus.2011.09.013.

[97] Y. Wu, Y. Lithwick, Density and Eccentricity of Kepler Planets, Ap. J. 772 (2013) 74. arXiv:1210.7810, doi:10.1088/0004-637X/772/1/74.

[98] H. Hussmann, F. Sohl, T. Spohn, Subsurface oceans and deep interiors of medium-sized outer planet satellites and large trans-neptunian objects, Icarus 185 (2006) 258–273. doi:10.1016/j.icarus.2006.06.005.

[99] D. Ehrenreich, A. Cassan, Are extrasolar oceans common throughout the Galaxy?, Astronomische Nachrichten 328 (2007) 789. arXiv:0704.3024, doi:10.1002/asna.200710798.